GWAS FOR MAIZE FUSARIUM EAR ROT RESISTANCE IDENTIFIES CANONICAL AND NON-CANONICAL PATHOGENESIS-RELATED GENES

A Thesis Presented for the

Master of Science

Degree

The University of Tennessee, Knoxville

Sanskriti Acharya

December 2025

ACKNOWLEDGEMENTS

I want to express my gratitude to my advisor, Dr. Bode Olukolu, for his guidance and support throughout this project. I am also grateful to my committee members, Dr. Heather Kelly and Dr. Gayan Kariyawasam, for their contributions of expertise in their respective fields. I am grateful to Allison Adams and all the students and employees in the Olukolu lab for their help in conducting experiments. Thank you to my parents, Mahesh Kumar Acharya, and Sarita Subedi, for their constant wisdom and guidance. Most importantly, thank you to my husband, Pawan, for his continued love and support.

ABSTRACT

Fusarium ear rot (FER), caused by *Fusarium verticillioides*, lowers grain quality and market value and contaminates kernels with carcinogenic fumonisins. Chemical and cultural controls are inconsistent, and genetic resistance is complex and environment dependent. We integrated multi-environment field phenotyping (2020–2021), genome-wide association studies (mixed models on whole-genome variants), and microbiome-aware heritability modeling in a panel of 272 diverse maize inbreds evaluated under natural infection (NI) and artificial inoculation. The composite FER index aligned most strongly with NI, indicating related but distinct resistance components under the two pressures. GWAS detected 28 significant SNPs across 14 loci on chromosomes 1, 2, 3, 6, 9, and 10. Canonical candidates included an RPM1-interacting protein (RIN-family; RIN13), an AP2/ERF transcription factor, a cytochrome P450, and Villin-4, implicating immune signaling, hormone-mediated defense, detoxification, and cytoskeletal remodeling. Non-canonical, defense-linked candidates PFK1, sucrose-phosphate synthase–like (SPS), malic enzyme 15, a vitamin B6 enzyme, triacylglycerol lipase 1, SNF1-related kinase (KIN11-like), a P4-type phospholipid-transporting ATPase, YSL6 metal–nicotianamine transporter, and an ornithine cyclodeaminase/μ-crystallin–family gene highlight roles for energy/carbon metabolism, redox buffering, membrane-lipid homeostasis, and micronutrient transport. At the association level, most signals are shared by FER and NI, with fewer unique to inoculation, supporting a two-step breeding approach: screen under inoculation to remove highly susceptible lines, then select under NI (or the NI-aligned composite) for durable, field-relevant resistance.

TABLE OF CONTENTS

CHAPTER ONE

LITERATURE REVIEW

Maize

Maize (*Zea mays*) is an important cereal crop in the U.S. and globally, significantly impacting agriculture and the economy (Arata et al., 2024). In 2024, the United States produced 14.9 billion bushels of corn, generating a production value of about $64.7 billion, which placed maize well ahead of other major staples such as soybeans ($44.1 billion), all hay ($18.6 billion), all wheat ($10.9 billion), cotton ($4.67 billion), rice ($3.43 billion), and tobacco ($0.78 billion) (U.S. Department of Agriculture, National Agricultural Statistics, USDA, 2025, Crop Production 2024 Summary; USDA NASS, 2025, Crop Values 2024 Summary). Apart from its role in domestic production, corn was also a top U.S. export in 2024, valued at $13.7 billion compared with $24.47 billion for soybeans, making it important to farm income and downstream industries such as feed and ethanol (U.S. Department of Agriculture, Foreign Agricultural Service, USDA, 2024). At the global level, maize ranks among the most valuable agricultural commodities, with exports totaling $45.5 billion in 2024.

Beyond economics, maize is important as a food source, livestock feed, and a raw material for biofuels and bioplastics, while also contributing to soil health through crop rotation (Erenstein et al., 2022). Maize-based systems improve soil conditions when crop residues are retained, cover crops are integrated, and tillage is reduced. These practices protect against erosion, enhance water infiltration, and aggregate stability, and sustain soil microbial communities, thereby strengthening soil structure and nutrient cycling (Basche et al., 2019).

Despite its central role, maize production remains vulnerable to environmental stress. In the 2022/23 season, U.S. maize output fell to 346.74 million metric tons from 386.60 million metric tons in 2021 due to adverse weather, changing agricultural practices, and fungal diseases (USDA; Du, S., & Xiong, 2024; Rajath et al., 2023; Ma et al., 2024).

Fusarium Ear Rot in Maize

Fusarium spp. are among the most damaging fungal pathogens, affecting maize both in the field and during storage. These fungi infect plants through wounds, often caused by insects, and thrive under favorable environmental conditions, producing harmful mycotoxins such as fumonisins, zearalenone, and trichothecenes (Solórzano-Solórzano et al., 2024). These toxins disrupt cellular processes, weaken plant defenses, and promote fungal colonization (Perochon et al., 2024). In storage, high moisture and temperature further enhance *Fusarium* growth, increasing mycotoxin contamination (Lee et al., 2015). The main *Fusarium*-related diseases include stalk rot, pink rot, and Fusarium ear rot (FER), all of which threaten yield and grain quality (Czembor et al., 2015). FER, primarily caused by *Fusarium* verticillioides, is one of the most prevalent and destructive diseases affecting maize. Although its impact on yield may not always be severe, the main concern is the contamination of maize with fumonisins (Gamanya et al., 2001). F. verticillioides produces a variety of secondary metabolites, including fusaric acid, fusarins, and fumonisins, with fumonisins being the most abundant in infected kernels. The disease thrives in warm to hot, dry conditions, particularly during silking and grain filling. Drought-stressed plants exhibit weakened defenses and are more susceptible to insect feeding, which further heightens the risk of infection (Licht et al., 2017). While initial infection flourishes

in dry conditions, subsequent humid or wet weather near harvest can worsen fungal growth and mycotoxin accumulation. Prolonged periods of rainfall that delay harvest significantly raise the risk of contamination, showing the necessity for timely disease control. Maize planted later in the season often experiences more severe FER and higher fumonisin concentrations (Parsons et al., 2010). Although this is largely associated with heat and drought stress during silking, other contributing factors include increased pressure from ear- and kernel-feeding insect pests, particularly corn earworm (*Helicoverpa zea*) and western bean cutworm (*Striacosta albicosta*) accumulation (Dragich & Nelson, 2014; Eichenseer et al., 2014), which create wounds that facilitate colonization by *F. verticillioides*, can vector pathogens when they infest corn ears or contact corn silks, and substantially elevate fumonisin levels, resulting in greater disease severity and more substantial fumonisin.

Between 2012 and 2023, Fusarium ear rot fungi were estimated to have decreased maize yields by around 1.9 billion bushels, equating to financial losses of approximately $8.6 billion (USD Crop Protection Network, 2024). In 2023, Fusarium ear rot caused significant damage, resulting in an estimated loss of 46.9 million bushels across 29 major corn-producing states in the U.S. (USDA Crop Protection Network, 2024). In the growing season of 2024, Fusarium ear rot losses increased to an estimated 53.6 million bushels across the same states (USDA Crop Protection Network). This disease impacts maize yield and also compromises grain quality, often resulting in substantial financial losses even when the harvested grain appears normal and asymptomatic. Contaminated kernels frequently harbor mycotoxins, which can lead to shipment rejections and decreased market value, ultimately affecting farmers' profitability.

Despite its scale and the mycotoxin risk, there is no consistently effective, chemical-based management for FER. The main concern is fumonisin accumulation in grain colonized by *F. verticillioides*, with regulatory guidance allowing only low ppm levels in food and species-specific limits in feed. Drought, heat stress, and insect injury can accumulate on ears resulting in higher fumonisin and related mycotoxin loads. Only a few foliar fungicides such as prothioconazole (Prolin 480 SC) or premix products like Miravis Neo are occasionally labeled for ear rots (Woloshuk & Wise, 2014), but field efficacy for FER has not been demonstrated, and extension guidance suggests that sprays generally have little impact compared with practices that limit ear wounds from insects, timely harvest, and proper grain drying. (U.S. Environmental Protection Agency, 2015; Syngenta Crop Protection, LLC, 2023). By contrast, aflatoxin produced by *Aspergillus flavus*, another ear-rot fungus in maize, can be mitigated in some regions with atoxigenic biocontrol products such as AflaGuard (an atoxigenic *A. flavus* strain), which is registered as a microbial pesticide to displace aflatoxin-producing strains (Bowen & Hagan), but these do not address fumonisin contamination and underline the gap in analogous tools for FER. Multiple field studies report that foliar fungicides or elicitors applied around silking do not reliably reduce FER symptoms or fumonisin contamination. Some show no ear-disease effect at all, and in some cases, prophylactic spray programs failed to lower FER and did not consistently reduce mycotoxin levels (Janse van Rensburg et al., 2016; Blandino et al., 2022).

At the same time, breeding durable resistance is difficult. FER resistance in maize is quantitative and polygenic, with strong genotype and environment interactions that cause hybrid

rankings to shift across sites and years. There is no complete immune resistance, and progress is often incremental (Lanubile et al., 2017). In practice, most programs and seed companies screen and rate hybrids for lower susceptibility tolerance rather than claiming intentionally bred, high, race-stable resistance to *F. verticillioides.* Growers are advised to select hybrids with better ear-rot scores and pair that choice with insect management and cultural practices (Crop Protection Network, 2024).

Given these challenges, implementing effective disease management strategies is essential to minimizing *Fusarium*-related losses and ensuring the safety and sustainability of maize production.

Impact of cultural practices on FER Incidence and severity

Efforts to mitigate Fusarium ear rot have encompassed various strategies, including cultural practices, biological control, chemical treatments, and genetic improvements (Masiello et. al., 2019, Munkvold et al.,2003, Cavaglieri et al.,2004). Among cultural practices, crop rotation and residue management play an important role in reducing fungal inoculum in fields, while timely harvest and proper post-harvest storage conditions help minimize fungal growth and mycotoxin accumulation in grains. Tillage practices also influence Fusarium ear rot incidence by affecting the survival and distribution of fungal inoculum. In the study by Skoglund et al. (1988), when high levels of naturally occurring inoculum coincide with favorable environmental conditions, the pathogen can overcome plant resistance and tillage-related benefits, making genetic resistance and agronomic practices ineffective. However, in years of low infection, tillage practices may influence disease incidence and yield, offering a potential management

strategy. The ability to assess the true impact of tillage on disease control is limited by naturally occurring inoculum, which masks treatment effects and prevents the use of a pathogen-free control for evaluation. *Fusarium* spp. overwinter in maize stubble, and its persistence depends on residue placement (Flett et al., 1998). Conservation tillage or no-till, which retains crop residues on the soil surface, promotes the survival of *Fusarium* inoculum, increasing the risk of infection in subsequent maize crops. In contrast, conventional tillage, such as deep plowing, buries infected residues, accelerating decomposition and reducing inoculum levels. Therefore, tillage selection should be integrated with other management strategies to effectively control Fusarium ear rot and minimize its impact on maize production. Biological control agents, including *Trichoderma* spp. and Bacillus-based products, have shown potential in suppressing fungal proliferation and reducing mycotoxin levels in field trials. Chemical fungicides, though limited in effectiveness, are occasionally employed during high-risk periods to provide supplementary control (Solórzano-Solórzano et al., 2024).

Breeding Approaches and Genetics

Among the various methods for managing FER in maize, genetic approaches have gained attention due to their potential for sustainable disease management. The preferred approach for controlling *F. verticillioides* infections and reducing mycotoxin levels is to breed resistant maize cultivars (Gaikpa et al., 2019). Identifying resistant genotypes remains a priority, as genetically resistant hybrids offer an environmentally safe approach to disease management (Munkvold et al., 2003). A valuable resource for resistance breeding is the maize inbred diversity panel, which consists of genetically diverse maize lines used to study trait variation and identify resistance

sources. In the late 1990s, Major Goodman selected a panel of 282 maize breeding lines representing temperate, tropical, sweet corn, and popcorn varieties despite limited genotyping technology at the time. Decades later, this panel has become highly valuable for diversity and mapping studies within the maize research community (Flint-Garcia et al., 2005). This panel allows genome-wide association studies (GWAS), helping pinpoint loci linked to FER resistance and fumonisin accumulation. Screening inbred lines under controlled and field conditions can potentially allow researchers to integrate natural resistance alleles into breeding programs. Breeding programs have identified sources of resistance to FER, yet few commercial hybrids currently possess high levels of resistance. Modern genomic tools are addressing this gap effectively. GWAS studies have identified significant single nucleotide polymorphisms (SNPs) and genes involved in critical defense mechanisms, including transcription factors, cytochrome P450 enzymes, ubiquitination proteins, and chitinases (Li et al., 2024; Stagnati et al., 2019).

Prior studies rarely look into natural vs. artificial infection in the same panel and seasons. Inoculation methods and multi-environmental trials can change correlations with FER disease severity and shift the molecular gene pathways that appear important. Comparing both treatments in parallel is necessary to understand which signals can be generalized to farmer-relevant disease pressure (Butoto et al.,2021; Mesterhazy et al.,2022). By using whole-genome sequence variants, we can use very high marker density, improving mapping resolution and reducing reliance on imputation after applying stringent filtering thresholds in these maize genomes that show huge structural variants and presence/absence variation (Bukowski et al., 2018). Conventional GWAS and heritability estimation generally ignore the role of the host-

associated microbiome, even though microbial communities and interactions influence plant stress responses, pathogen virulence, and disease outcomes (Yang et al., 2024). In this study, microbiome features are used to model epistasis with host genetic variants to refine heritability estimates, helping to account for part of the missing heritability in Fusarium ear rot resistance. This integrative approach, combining artificial and natural infection trials, contrasting years including a no-till season, whole genome sequencing (WGS) variants, and microbiome-informed heritability analysis, distinguishes this study from earlier FER mapping efforts and addresses limitations that have hindered durable progress.

Addressing FER through conventional breeding is further complicated by low to moderate heritability under single-environment testing. Multi-environment trials and mixed-model Best Linear Unbiased Prediction (BLUPs) are required to partition environmental noise, raise effective heritability, and obtain stable breeding values (Schmidt et al., 2019). Because FER resistance is governed by many small-effect loci, focusing on a handful of quantitative trait locus (QTL) has not produced durable gains. This also explains why many environment-specific QTL fail to translate across populations, reinforcing the need to emphasize high-resolution mapping and careful modeling of genotype and environment interactions, rather than relying on single-locus approaches. Nevertheless, GWAS allows for understanding the complexity, various gene pathways, and genetic architecture that drive phenotypic expression.

This study hypothesizes that FER resistance is strongly shaped by environmental factors, which lowers heritability when measured under a single environment. To test this, we phenotyped across multiple environments (2020,2021) and inoculation types, analyzing natural

infection and artificial inoculation in the same panel and applying a cocktail containing 45 *Fusarium* isolates to capture diverse virulence. We further hypothesize that, because FER resistance is polygenic with many small-effect loci, explicitly modeling genotype × environment interactions is required to obtain stable heritability estimates (Lanubile et al., 2017; Santiago et al., 2020). We also hypothesize that the host-associated microbiome contributes to observed modulation of resistance, and by fitting variance-partitioning models that include host genomic relationship matrix, relationship matrices based on microbial relative abundances, and host × microbiome interactions (GxGxM), we can refine heritability estimates and attribute the share explained by microbiome terms. Prior evidence that maize genotypes shape heritable microbiome features and that the microbiome in turn impacts phenotypic expression supports this expectation (Walters et al., 2018; Wagner et al.,2022).

Finally, we hypothesize that GWAS using WGS derived SNP and insertion or deletion (INDEL) variants will identify biologically significant loci underlying FER resistance and improve mapping resolution (Bukowski et al., 2018; Wang et al., 2024). Compared with earlier studies, we expect that avoiding marker imputation in these genetically diverse, unrelated inbreds will reduce the noise-to-signal ratio during GWAS. Together, these hypotheses frame a design that clarifies the genetic architecture of FER resistance under farmer-relevant disease pressure, where natural and artificial challenges may alter which, loci appear important and produce more robust heritability estimates that integrate both host genetics and the metagenome.

Rationale and Significance

Fusarium ear rot (FER) resistance in maize is controlled by many small genes and is strongly influenced by the environment, so resistance can look different across years and locations. GWAS in diverse panels are preferred since they provide finer resolution and account for population structure (Lanubile et al., 2017; Santiago et al., 2020; Korte & Farlow, 2013). Treatment methods also matter since natural and artificial inoculations can give different results, so testing both simultaneously in the same panel and seasons is important (Butoto et al., 2021; Mesterházy et al., 2022). Finally, analyzing data across multiple environments with mixed linear models that test both additive and dominance genetic effects allows for more robust estimation of genetic contributions to trait variation (Schmidt et al., 2019). While most traits are expected to be primarily influenced by additive effects, including dominance effects can capture additional genetic variation, particularly for traits where non-additive interactions contribute substantially to phenotypic variation.

In this study, we phenotype a single maize diversity panel under both natural infection and artificial inoculation across two years (2020 and 2021, including a no-till season) using a cocktail of 45 *Fusarium* isolates. This design mimics farmer-relevant disease pressure while allowing side-by-side comparisons of infection methods (Butoto et al., 2021; Mesterházy et al., 2022). We first analyze FER phenotypes to characterize natural variation in the population. We then estimate trait heritability to see how much of the observed variation is genetic versus environmental, and refine those estimates by incorporating multi-environment data as well as host-associated microbiome features. Prior work shows maize genotypes harbor heritable

rhizosphere taxa, so our variance-partitioning models include kernels derived from host genome, host-associated microbiome, and host × microbiome interactions (GxGxM) to better capture the full heritable component of FER resistance (Walters et al., 2018; Wagner et al.,2022).

On the genotyping side, we use whole-genome sequencing to increase mapping resolution and minimize imputation compared with older, mid-density marker sets (Bukowski et al., 2018). We then use GWAS to detect genomic regions and specific candidate genes linked to FER resistance, interpreting those signals with functional annotations to judge biological plausibility. To understand stability, we examine environmental effects through G×E analysis and evaluate whether resistant genotypes remain consistently resistant across sites and seasons.

By combining multi-environment phenotyping, including natural and artificial infection, high-density WGS, and microbiome-aware heritability modeling, this study aims to provide more stable heritability estimates for FER resistance, identify biologically meaningful loci with improved resolution through GWAS for subsequent functional follow-up, and establish a framework that can be applied to study other complex, environment-dependent diseases in maize and other crops. This research provides insights that can guide breeding programs globally, supporting more resilient and sustainable maize production under diverse and changing climates.

CHAPTER TWO

INTRODUCTION

Genome-wide association studies

GWAS uses natural diversity and past recombination to pinpoint DNA regions linked to complex traits like FER. Maize is well-suited for GWAS because linkage disequilibrium (LD) decays quickly, often within less than a kilobase scale to a few kilobases (Olukolu et al., 2013; Zuffo et al., 2022), so that the signals can be mapped at single-gene resolution, though this requires high-density markers (Yan et al., 2009; Wallace et al., 2014). A practical complication is that many small-effect loci contribute to FER resistance, so single SNPs explain little variance, and results are more reliable when designs use multiple environments to differentiate stable and unstable causal loci (Korte et al., 2013).

To avoid false positives due to population structure and relatedness (e.g., tropical vs. temperate groups), modern plant GWAS uses mixed linear models (MLM) that include a kinship matrix and optional covariates like principal components (or ancestral relatedness from STRUCTURE analysis) to yield better-calibrated p-values (Yu et al., 2006; Alamin et al., 2022). Computational refinements such as compressed MLM and P3D/EMMAX estimate variance components once or group similar lines and allow genome-wide scans with hundreds of thousands of SNPs, feasible with little loss of power. These approaches are implemented in tools like GAPIT and GWASpoly (Zhang et al., 2010; Kang et al., 2010).

Kinship Matrix Construction

For mixed-model GWAS, the kinship or genomic relationship matrix (K) is computed from SNPs and not pedigrees to capture realized genetic relatedness. A standard approach is VanRaden's method, which (genotypes coded as 0, 1, and 2) centers by allele frequency and scales the cross-product so diagonals approximate inbreeding and off-diagonals reflect pairwise relatedness. This construction is widely used in GWAS/GBLUP across plant and animal systems (VanRaden, P. M, 2008; Forni et al., 2011). In diverse or multi-population panels, the unweighted Method 1 is commonly preferred for stability and straightforward interpretation, and Method 2 down-weights common alleles (Wientjes et al., 2017). In practice, marker-based K remains standard in plant pipelines and software (e.g., GAPIT; AGHmatrix), providing the random-effect term in MLMs that controls population stratification and cryptic relatedness (Gianola et al.,2016).

GWAS Software and Tools

Common GWAS tools include TASSEL, GAPIT, and GWASpoly. TASSEL provides baseline GLM and MLM association tests widely used in maize genetics (Bradbury et al., 2007). GAPIT (v3) extends mixed-model GWAS with faster, higher-power multi-locus methods such as MLMM, FarmCPU, BLINK, and SUPER, while retaining standard MLM and CMLM workflows (Wang et al., 2021). GWASpoly, designed for autopolyploids, is also applied to diploids and is used for testing non-additive gene actions (e.g., additive; dominance models such as 1-dom-ref, 1-dom-alt; and dosage-based models in polyploids) within a mixed-model framework (Rosyara et al., 2016). Across these platforms, mixed models with a kinship matrix

are routine to control population structure or relatedness, and computational accelerations like compressed MLM and P3D/EMMAX make genome-wide scans practical at high marker density (Zhang et al., 2010).

GWAS and Genomic Approaches to FER Resistance in Maize

Previous genetic studies of FER resistance in maize consistently indicate that resistance is quantitatively controlled by many loci, each contributing a small to moderate effect. Early quantitative trait locus (QTL) mapping in biparental populations found several QTL with relatively small effects, and these tended to be inconsistent across different genetic backgrounds or environments (e.g., a QTL detected in one family might not segregate in another). The advent of GWAS, which surveys much broader genetic diversity, provided a more detailed picture of this polygenic architecture. Zila *et al.* (2014) conducted GWAS on FER resistance using a panel of 1,687 diverse U.S. maize inbreds from a core diversity panel representing global maize diversity. They identified seven SNPs significantly associated with FER resistance, each SNP accounting for only 1–3% of the phenotypic variance. The favorable alleles at these loci and alleles associated with reduced ear rot and lower fumonisin levels were rare in the overall panel, often with frequencies below 0.16 and more prevalent in tropical germplasm than in temperate lines. This suggests that some useful resistance alleles exist in tropical maize that could be introgressed into temperate breeding material. However, because each locus had such a small effect, the authors concluded that marker-assisted selection on those individual SNPs would have a limited impact on improving resistance. Instead, they suggested that *stacking* multiple favorable alleles (pyramiding the small-effect QTL) and employing genomic selection to capture

the polygenic background would likely be more beneficial for enhancing FER resistance. In other words, because resistance involves many genes, a holistic genome-wide selection approach might outperform trying to chase a few minor QTL.

Subsequent studies have built on this finding and tried to further elucidate the biological pathways involved in FER resistance. A notable approach has been to combine GWAS with transcriptomic analysis to filter and prioritize candidate genes. Yao *et al.* (2020) performed GWAS on FER resistance in a Chinese maize panel under multiple environments and identified 34 significant SNPs, then integrated this with RNA-seq profiles of infected versus uninfected ears from resistant and susceptible lines. By comparing transcriptomes of the most resistant vs. most susceptible lines during early infection, they found hundreds of differentially expressed genes (DEGs) enriched in defense-related pathways such as plant hormone signaling (jasmonic acid, ethylene, etc.), phenylpropanoid biosynthesis, and detoxification enzymes (e.g., cytochrome P450s). They noticed that about 25% of the GWAS-identified candidate genes overlapped with DEGs from the transcriptome study. These overlapping genes make especially compelling candidates, as they are supported by both genetic association and inducible expression under *Fusarium* attack. Yao *et al.* showed several candidate defense genes from this combined analysis, including a MAP kinase gene, a pathogenesis-related protein 5 receptor-like kinase (PR5-like RK), heat shock proteins, and genes involved in hormone pathways. Their findings suggest that resistant maize lines respond to *Fusarium* infection by quickly activating immune signaling and metabolic pathways that strengthen cell walls or produce antifungal compounds, thereby limiting the pathogen's spread. This integrated GWAS transcriptomics

strategy exemplifies how functional genomic evidence can help prioritize which among many GWAS hits are likely to be biologically meaningful in conferring resistance.

Another recent study by Ayesiga *et al.* (2024) focused on tropical maize germplasm (151 inbreds) and applied both GWAS and pathway analysis to FER resistance. They detected seven significant SNPs on chromosomes 1, 2, 4, 5, and 9 that were associated with FER resistance in their panel, each explaining between 4% and 11% of the phenotypic variance. These values might be inflated due to the relatively small population size. While some of these per-locus effects are slightly larger than those in the Zila *et al.* study, they are still in the small to moderate range, reinforcing that no single major resistance gene dominates. The seven significant SNPs in the tropical panel were annotated to four putative genes (Zinc ion binding, Serine-type endopeptidase activity, monolayer-surrounded lipid storage body, and Protein peptidyl-prolyl isomerization). To gain insight into the polygenic network underlying resistance, the authors employed a pathway association analysis (using tools like PASTool). This analysis identified seven metabolic or signaling pathways that were enriched for genes associated with FER resistance in the tropical panel. The most significant pathway was the glyoxylate cycle, which is related to primary metabolism and possibly stress response.

The prior studies support a comprehensive approach to improving FER resistance. For GWAS analysis, it is important to test phenotypes across multiple environments or years to ensure that the detected QTL is robust to environmental variation. Many small-effect loci might only be detectable under certain environmental conditions (e.g., specific pathogen pressures or weather that accentuates differences), so multi-environment trials can help in capturing a fuller

spectrum of resistance alleles. Careful statistical calibration of the GWAS model is needed. Using MLMs with kinship and checking Q–Q plots (λ close to 1) helps avoid false positives that waste effort in validation. Finally, integrating functional evidence (such as gene expression data, known gene annotations, or pathway enrichment) when interpreting GWAS results greatly enhances the ability to identify true causal genes among the many linked markers. In our analysis of FER resistance, we heed these lessons by evaluating the panel in two years (with inoculated and non-inoculated trials), using a mixed model GWAS with kinship (VanRaden-based K) and P3D for stable variance component estimation, and by comparing our top GWAS hits with previously reported candidate genes from earlier FER studies. By doing so, we aim to focus on loci that not only shows statistical associations but also make biological sense in the context of maize's defense responses to *Fusarium*. The result is the identification of several loci with reproducible though small effects, and the nomination of plausible candidate genes near those loci. For example, genes involved in plant hormone signaling or antifungal pathways have been implicated by prior research.

This thesis applies multi-environment GWAS in the Goodman panel (2020–2021; inoculated and natural infection) to describe FER's polygenic architecture, compare NI and inoculated responses and their relation to the composite index, and identify reproducible small-effect loci with nearby candidate genes using gene annotations and prior reports.

Materials and methods

Plant material

The Major Goodman maize diversity panel, also known as the Maize 282 Association Mapping Panel, is a globally sourced collection of maize germplasm used extensively for genetic research (Flint-Garcia et al., 2005). We screened FER in 272 genotyped inbred lines from the 282 Goodman panel lines at one location, ETREC in Knoxville, TN, during 2020 and 2021. The 2020 and 2021 trials were at 35°53′45″N, 83°57′38″W and 35°53′51″N, 83°57′38″W, respectively; and seeds were sown in the second week of June in both years.

Experimental Design

All trials were planted using an augmented randomized complete block design comprising six blocks, six check replications, and two treatment conditions: inoculated (artificial infection; Inoc) and non-inoculated (natural infection; NI). Each experimental unit was a single-row plot measuring 9 ft × 2.5 ft (2.7432 m × 0.762 m) and contained 10 plants. Because most plots contained distinct inbred lines, each block included eight check plots (i.e., B73, B97, CML52, CML69, IL14H, MO17, NC358, and Tzi8) to assess block performance. Irrigation was supplied via a sprinkler system. At ETREC in 2021, planting occurred in no-till fields; while in 2020 at ETREC, planting was in tilled fields. All experiments were established on fields with a prior soybean crop. To minimize edge effects, the maize variety Purple B73 was planted as border rows in two-row plots.

Inoculation

Within each plot, half of the plants were inoculated while the remaining half served as non-inoculated controls. Inoculations were performed 10 days after silking. Toothpicks were coated with a cocktail containing 45 Fusarium isolates. For each plant, one toothpick was inserted into the side of the ear (cob), and a second toothpick was inserted through the silk channel.

FER Rating	1	2	3	4	5	6	7
Genotype	CML61	NC362	Tzi8	NC306	K148	CML52	A214N

Figure 1 Visual scale for FER severity in maize ears (1–7, resistant to susceptible) with representative genotypes (CML61, NC362, Tzi8, NC306, K148, CML52, A214N); higher scores indicate greater *rot* coverage and fewer sound kernels, reflecting that inbred seed set can vary, so severity is evaluated by both the extent of rot and the number of intact kernels.

Sample Collection and Phenotypic Data

At physiological maturity, three ears were harvested from each of the inoculated and non-inoculated subsets of plots. Ears were photographed and visually rated for FER severity on a 1–7 scale (1 = least severe; Figure 1; Landry Adams 2022). Following the rating, kernels were

collected in Falcon tubes for DNA extraction of kernel-associated metagenomes using the kernel wash method. The phenotypic traits considered in the analysis included NI_2020, NI_2021, Inoc_2020, Inoc_2021, NI, Inoc, and FER. The BLUE (or LSmeans) values were computed with a mixed linear model, where inbred lines were fitted as fixed effects and blocking, environment (year), treatment, and treatment-by-environment effects were fitted as random effects.

Kernel Wash and Microbiome Extraction

To extract the kernel-associated microbiome, 10 mL of ddH_2O was added to each Falcon tube containing the harvested kernels and shaken vigorously for 10 minutes. Kernels and debris were removed, retaining the liquid. The suspension was centrifuged at 4 °C, 3220 rcf for 5 minutes, and the supernatant was discarded. The pellet was resuspended in 20 µL of 20% glycerol, vortexed, and stored in 96-well deep-well plates at −80 °C until DNA extraction was performed.

DNA Extraction

For DNA isolation, the plate was thawed and centrifuged at 4000 rpm for 30 minutes. After removing the supernatant, 500 µL of 2× extraction buffer supplemented with 30 µL freshly prepared lysozyme (10 mg/mL), 15 µL proteinase K (4 mg/mL), and 2 µL RNase A (10 mg/mL) was added to each well. The mixture was gently inverted and incubated at 65 °C for 30 minutes, then centrifuged at room temperature for 30 minutes at 4000 rpm. The supernatant was carefully transferred to a fresh 96-well plate, avoiding any white precipitate. One-half volume of PEG 8000/MgCl was added to each sample and incubated at room temperature for 1–2 hours. DNA was pelleted by centrifugation at 4000 rpm for 30 minutes at room temperature. The supernatant

was removed, and residual liquid was aspirated. Pellets were resuspended in 400 µL TE buffer (containing RNase A at 20 µg/mL) and incubated at 65 °C for 15 minutes. For further purification, an equal volume of chloroform-isoamyl alcohol was added, the tubes were inverted for 2 minutes and centrifuged at 4000 rpm for 30 minutes at room temperature. The upper aqueous phase was transferred to a clean tube, mixed with 0.1 volume of 5 M NaCl, followed by 2.5× volumes of 100% ethanol. Samples were gently inverted and centrifuged at 4000 rpm for 30 minutes at room temperature to pellet the DNA. Pellets were washed once with 70% ethanol, centrifuged at 4000 rpm for 30 minutes, and air-dried after decanting and aspirating 70% ethanol. Finally, DNA was dissolved in 30 µL TE buffer and stored at 4 °C until use.

OmeSeq-qRRS Library Construction and Sequencing

Library preparation followed the general workflow described by Kuster et al. (2021). OmeSeq-qRRS is a reduced-representation, genome-wide sequencing approach designed for both genotyping and metagenomic profiling at low cost. By capturing only, a subset of genomic regions within component genomes of the metagenome, this method addresses limitations common to amplicon-based and shotgun metagenomic approaches (Adams et al. 2023, 2024). The protocol consisted of the following main steps: (i) DNA quantification and normalization, (ii) Sequential double digestion and adapter integration (dual-barcoded adapters), (iii) size selection, and (iv) PCR amplification and final size selection.

DNA concentrations were measured with the Quant-iT PicoGreen dsDNA Assay Kit (Thermo Fisher Scientific), and samples were standardized to 20 ng/µL, with a lower bound of approximately 1 ng/µL when necessary. Genomic DNA was digested consecutively with NsiI-

HF and NlaIII (New England Biolabs). After each digestion, custom Illumina P5 and P7 adapters containing unique molecular identifiers and variable-length barcodes (7–10 bp; 96 × 96 combinations) were introduced. Each barcode was preceded by a 6-bp buffer to ensure placement within a high-quality read region. Only the 4-bp overhangs generated by the restriction enzymes facilitated annealing, maintaining double-stranded DNA, and minimizing off-target priming during isothermal amplification. Adapter incorporation and isothermal amplification were achieved sequentially after each digestion (NsiI-HF, and then NlaII), using the strand-displacement activity of Bst 2.0 WarmStart DNA Polymerase (New England Biolabs) under isothermal conditions. A double-sided AMPure XP MagBead (Beckman Coulter) step enriched for fragments approximately 300–800 bp in length (includes flanking adapter regions of 75 bp on each side). Libraries were amplified by quantitative PCR (18 cycles), followed by a second double-sided size selection to retain fragments within the 300–800 bp range. Pooled libraries were then sequenced on an Illumina NovaSeq 6000 S4 flow cell at the Genomic Sciences Laboratory, North Carolina State University.

Demultiplexing and Read Processing

Raw sequencing data were processed with ngsComposer (Kuster et al. 2021). Quality control and demultiplexing parameters included: (i) removal of the 6-bp buffer preceding each barcode, (ii) assignment of reads allowing a maximum of one mismatch across the 7-10 bp variable length barcodes (implemented with the edit/levenshtein distance method that accounts for both substitutions and indels), (iii) Filtering reads based on intact restriction site motifs, (iii) trimming with a sliding 10-bp window requiring a minimum base quality score of Q20, (iv)

enforcing a minimum post-trim read length of 32 bp, (v) adapter removal based on at least 12 bp of sequence matching, and (vi) Retention of reads with a Phred score ≥20 across at least 80% of the read.

Metagenomic Profiling

Microbial community profiling was conducted using the Qmatey pipeline, which applies an exact-matching strategy for high-resolution taxonomic classification at the strain level and uses consensus sequence matching for higher taxonomic ranks (Adams et al. 2023; https://github.com/bodeolukolu/Qmatey). Unlike amplicon-based 16S or ITS sequencing, OmeSeq-qRRS allows phylum-to-strain level characterization across diverse microbial groups via reduced-representation metagenome sequencing. Reads attributed to the host genome were removed by aligning to the Zea mays B73 RefGen_v4 assembly using the Burrows-Wheeler Aligner (maximal exact match). The remaining unmapped reads were compressed, indexed, and aligned to the NCBI nucleotide database using Megablast. Exact matching enabled strain-level identification, while consensus-based matching supported assignments at species through phylum rank. Quantitative abundance tables, normalized by relative sum scaling, were generated at all taxonomic levels (Supplementary Files S2 and S3). The normalized species-level abundance was used as a metagenomic kernel for computing broad-sense heritability.

Genotypic Data Collection and Quality Control

Whole-genome variant data for the Goodman panel were obtained from previously published resequencing efforts (Bukowski et al., 2018). Briefly, raw reads were aligned to the B73 reference genome, and variant coordinates were subsequently lifted over to AGPv4. After

initial joint variant calling (>83 million unimputed SNPs and indels), markers were filtered to retain sites with minor allele frequency (MAF) ≥0.02, genotype read depth ≥6, and ≤20% missing data across either markers or samples. This produced a high-density marker set of 310,792 SNPs and short indels for analysis. Variant filtering was performed using the GBSapp pipeline (Rickman et al., 2025).

Linkage Disequilibrium

LD was quantified using 310,792 genome-wide markers scored across the panel. Pairwise LD between markers was calculated as the squared Pearson correlation coefficient (r^2) of allele dosages using the Hmisc package in R. To summarize genome-wide LD decay, marker pairs were binned by physical distance, and r^2 distributions were visualized by distance bin. A threshold of $r^2 = 0.1$ was used as a practical indicator of substantial linkage. For fine mapping around GWAS signals, local LD was examined up to 500 kb windows (Figure S3, S4, S5) centered on significantly associated markers. Heatmaps of local r^2 were used to evaluate whether the associated SNP was in high LD ($r^2 \geq 0.1$) with a single nearby gene or with multiple genes in extensive LD blocks. Regions in which LD decayed to essentially a single-gene span were considered to nominate a candidate gene. LD estimates between marker pairs were plotted against their physical positions based on the maize B73 reference genome assembly version 4.

Population structure analysis

Population structure was inferred using sparse nonnegative matrix factorization (sNMF) as implemented in the LEA R package (Frichot & François, 2015). Genotypes (0/1/2 alternate-allele dosage) at 310,792 markers were provided to the snmf () function, and we fit ancestry

models with K ranging from 1 to 10. For each K, 10 independent runs were performed to assess convergence.

Two complementary criteria were used to choose the number of ancestral groups. First, we inspected the cross-entropy score reported by LEA, which measures how well the model predicts masked genotypes. Lower values indicate a better fit, and K values at or near the minimum (i.e., the point after which additional K values gave only marginal improvement) were selected. Second, we examined the Evanno-style ΔK heuristic, which supports the strongest hierarchical split by identifying the K value with the largest change in model likelihood between consecutive K values. An agreement between these two approaches was used to define the final K, and we also visualized one additional ancestry component to highlight admixed lines.

Genome-wide association analysis

GWAS was performed in R using GWASpoly v2.12 (Rosyara et al., 2016). Association tests were run with a mixed linear model that accounts for both population structure and relatedness. The general model implemented was:

$$y = X\beta + ZS\tau + ZQv + Zu + \varepsilon$$

Where y is the vector of phenotypic observations; Xβ represents fixed effects (e.g., environmental covariates); Sτ represents marker effects under a specified dosage model; Qv captures subpopulation structure; is the vector of random polygenic effects with covariance proportional to the genomic relationship (kinship) matrix K; and ε is the residual error. Following Rosyara et al. (2016), the polygenic term u was modeled as u∼N (0, σ2gK), and residuals as ε∼N (0, $I\sigma^2\tau$). We generated Manhattan and QQ plots for each trait–model

combination and used the QQ plots to evaluate inflation/deflation of test statistics. Only models showing acceptable false-positive control (i.e., QQ plots with minimal early upward deflection) were considered further.

For each significant marker, we calculated the proportion of phenotypic variance explained (PVE) within the panel. Under an additive dosage model, PVE was estimated as:

$$PVE_{additive} = \frac{Var(SNP)}{total\ phenotypic\ variance} = \frac{2p_j\ x\ (1 - p_j)\ x\ \beta_j^2}{\sigma^2}$$

Where p_j is the allele frequency of the SNP, β_j is the estimated additive effect of that SNP from the GWAS model, and σ^2_y is the total phenotypic variance of the trait in the panel. For dominance models, the dominance effect estimate d_j replaced β_j, and the genotype variance term was $4p_j^2\ x\ (1 -\ p_j)^2$. For the dominance dosage model:

$$PVE_{dominance} = \frac{Var(SNP)}{total\ phenotypic\ variance} = \frac{4p_j^2\ x\ (1 -\ p_j)^2\ d_j^2}{\sigma^2}$$

Where d_j is the effect of the marker, and the term $4p_j^2\ x\ (1 -\ p_j)^2$ represents the expected variance due to heterozygosity at the locus.

Significance thresholds were defined using both the Bonferroni correction, which is conservative but minimizes false positives, and false discovery rate (FDR) (VanRaden, P.M., 2008), which is less stringent but more powerful. We also reported a suggestive cutoff of -$\log_{10}$P=5 for loci that did not pass Bonferroni but showed strong biological plausibility. All analyses were run in R version 4.4.1(Vitezica et al., 2013).

Identification of Candidate Genes

Physical positions of significantly associated markers were mapped to the B73 reference genome assembly version 4 (Wu et al., 2021). Genes located within the same LD block as a significant marker were considered as candidates if either (i) the variant fell within the gene body, (ii) within 3 kb upstream of the start codon (putative promoter region), or (iii) local LD ($r^2 \geq 0.1$) supporting a tight association between the marker and a single gene within less than 100 kb. When multiple genes are in LD with the associated marker, the gene with the closest proximity is selected and annotated as not being supported by local LD analysis. We didn't exclude these genes since LD can be significantly distorted in genomes with complex structural variation and rearrangement, like maize. Functional descriptions for candidate genes were taken from maize genome annotations and supplemented with homology-based annotations (including Arabidopsis thaliana orthologs) and BLAST (NCBI BLAST). The literature review was then used to evaluate whether gene function was consistent with known or plausible mechanisms of *Fusarium* resistance.

Results

Principal component analysis (PCA) biplot of FER severity across four environment-trait combinations (Inoc_2020, Inoc_2021, NI_2020, NI_2021) (Figure 2A) shows that the first principal component (PC1) explained 48.6% of the total phenotypic variance and the second principal component (PC2) explained 24.6%. Each environment is represented by a vector on the biplot. The inoculated trials Inoc_2020 and Inoc_2021 have vectors pointing in a different direction than the non-inoculated trials (NI_2020 and NI_2021), indicating clear separation of

these environments along the PCs. The two treatments (NI and Inoc) also appear slightly separated along the axes (to a lesser degree than by years), as seen by the relative orientation of vectors for the same treatment across years. In sum, the PCA vectors for the two years, in particular, are oriented in roughly distinct directions, reflecting the major axes of variation in the FER data (Figure 2A).

In the Pearson correlation matrix (Figure 2B) among eight traits, FER severity from each year under inoculation (Inoc_2020, Inoc_2021) and natural infection (NI_2020 and NI_2021), FER severity based on composite traits (FER, NI, Inoc, FER_2020, FER_2021) were shown to be all positively correlated to various extents.

The combined FER index (BLUEs across NI_2020, NI_2021, Inoc_2020, and Inoc_2021) tracks with both environments closely, but especially for natural infection (NI) (i.e., NI vs FER = 0.90, NI_2020 vs FER_2020 = 0.89, and NI_2021 vs FER_2021 = 0.88). Inoculated data also align well with the combined FER index but slightly lower (Inoc vs FER = 0.86, Inoc_2020 vs FER_2020 = 0.84, and Inoc_2021 vs FER_2021 = 0.81). The composite also correlated well with single-year FER (FER vs. FER_2020 = 0.81; FER vs. FER_2021 = 0.79), indicating it's a useful summary measure, while still revealing year- and treatment-specific differences that likely arise from environmental factors (e.g., field conditions and tillage) rather than genetics alone.Correlations between any inoculated-related trait and any NI-related trait are only moderate to low (0.20–0.58). For example, NI_2021 vs Inoc_2021 = 0.35, Inoc_2020 vs NI_2020 = 0.58, and NI_2021 vs Inoc_2020 = 0.24. This implies inoculation and natural infection capture overlapping but distinct resistance components and environmental effects, so

rankings would shift between disease-imposition modes. Given that NI vs FER is slightly higher than Inoc vs FER (0.90 vs 0.86) and the same year NI_2020 vs FER_2020 is very high (0.89), the combined FER index appears more influenced by NI in 2020.

The kernel density plots or ridge plots (Figure 2C) are observed for the FER phenotypic score distributions for each of the eight traits for each trait-year combination: NI2020, NI2021, Inoc2020, Inoc2021, plus pooled NI, Inoc, and FER overall. Each trait's distribution is unimodal or single-peaked. The inoculated traits (Inoc_2020 and Inoc_2021) have broader distributions that are shifted toward higher severity scores, indicating higher mean FER and greater variation under inoculation.

For natural infection (NI), the 2020 distribution is centered near zero with moderate spread, whereas NI_2021 appears to have a pronounced peak, narrow, and slightly negatively skewed and tight, with a small secondary bump showing overall milder NI in 2021, with a small susceptible subgroup. Such a shift suggests that the underlying disease severity distribution changed significantly. Most genotypes received similar phenotypic scores (i.e., low variability in disease severity). The narrow width implies low variance, i.e., the trait values were tightly clustered. The slight right skew indicates a small number of lines had relatively higher resistance (higher phenotypic scores), but the majority were more similar or moderately affected. This could reflect uniform disease pressure under natural conditions, perhaps due to consistent environmental exposure (all naturally infected plants surrounded by artificially inoculated plants that should provide uniform disease pressure across trials) or low overall infection levels. It might also indicate low discrimination power in the phenotyping.

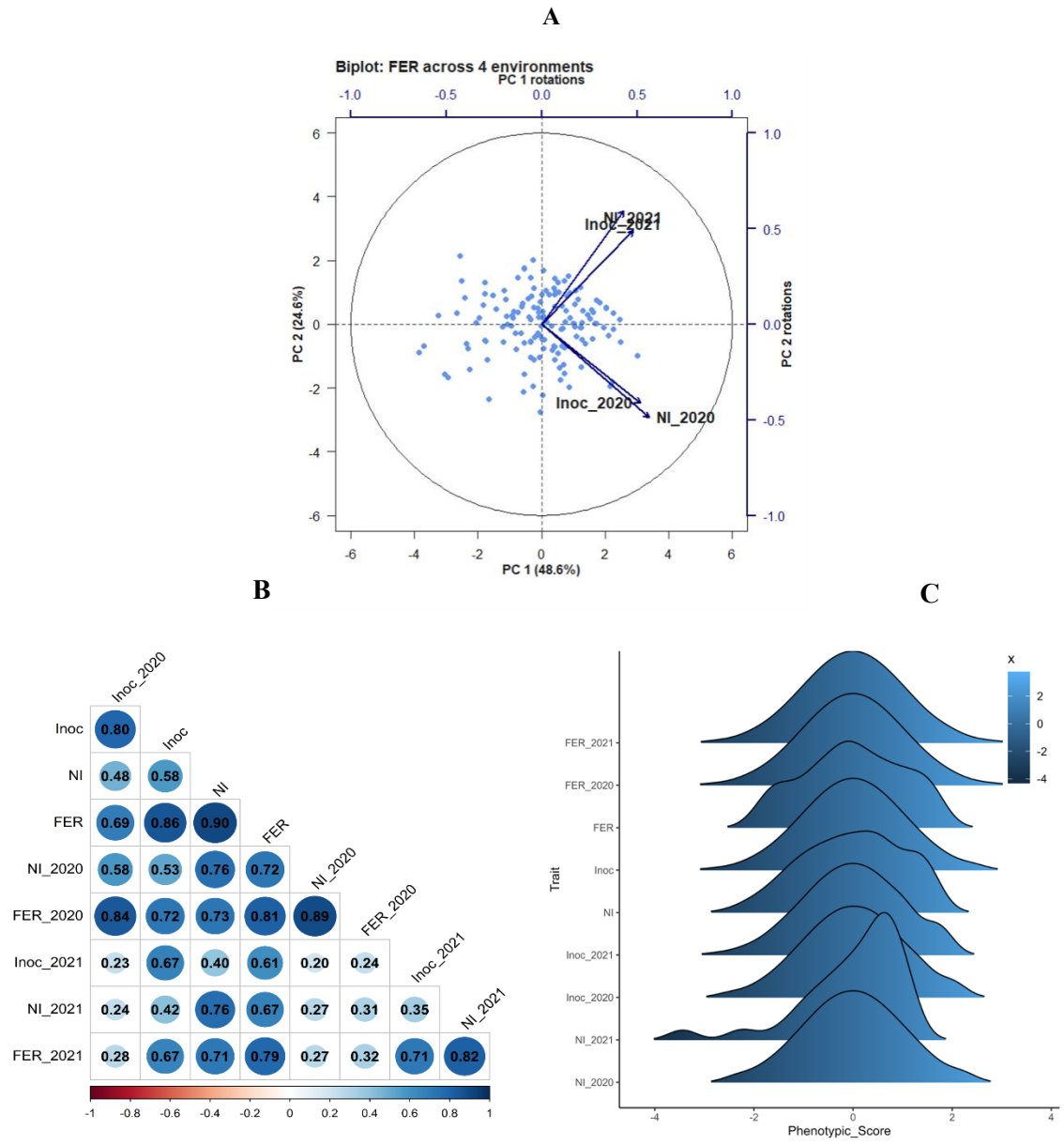

Figure 2 (A) Principal component analysis (PCA) biplot of FER severity across four environments (Inoc_2020, Inoc_2021, NI_2020, NI_2021). **(B)** Pairwise Pearson correlations among FER traits across environments, years, and composite indices. **(C)** Density distributions of FER phenotypic scores across inoculated, natural, and composite trait measures.

Inoc_2020 and Inoc_2021 are both right of zero with moderate spread, which shows that artificial inoculation produced consistently high pressure in both years. FER_2021 is slightly shifted to the right of FER_2020, FER, Inoc, and NI sit between their single-year counterparts, as expected for composites.

2021 NI was lighter (negatively skewed, tight). That pattern means realized epidemic intensity and/or microclimate in 2021 outweighed any residue-borne inoculum advantage expected under no-till. Tillage alone doesn't determine rankings, but year effects, weather, residue load, insects, and plot microclimate can flip the realized NI pressure. Therefore, NI and Inoc correlations vary by year, and FER is pulled closer to NI overall.

Table 1. Summary statistics of Fusarium Ear Rot (FER) phenotypes across inoculated and natural-infection (NI) trials and years (2020–2021), showing N, mean, SD, median, min, max, skewness, kurtosis, SE, and broad-sense heritability (H^2).

Traits	*N*	*Mean*	*Sd*	*Median*	*Min*	*Max*	*Skew*	*Kurtosis*	*Se*	H^2	h^2	$H^{2(GxM)}$
FER	273	4.76	1.58	4.73	1.47	7.77	-0.08	-0.92	0.10	0.61	0.49	0.83
Inoc	264	5.42	1.84	5.66	1.23	7.94	-0.44	-1.01	0.11	0.52	0.39	0.54
NI	268	4.13	1.79	3.99	0.30	7.79	0.09	-0.95	0.11	0.39	0.29	0.43
FER 2020	259	4.60	1.86	4.54	0.88	8.12	0.02	-1.22	0.12	0.71	0.61	0.71
FER 2021	218	4.68	1.85	4.70	0.10	7.99	-0.27	-0.87	0.13	0.62	0.57	0.75
Inoc 2020	240	5.24	2.10	5.60	1.14	7.71	-0.38	-1.37	0.14	0.28	0.51	0.31

Table 1: Continued

Traits	*N*	*Mean*	*Sd*	*Median*	*Min*	*Max*	*Skew*	*Kurtosis*	*Se*	H^2	h^2	$H^{2(GxM)}$
Inoc 2021	188	5.00	1.95	5.08	0.81	7.17	-0.50	-1.02	0.14	0.50	0.50	0.56
NI 2020	253	4.00	2.07	3.34	0.83	7.47	0.32	-1.33	0.13	0.33	0.35	0.36
NI 2021	202	4.42	2.23	4.45	-0.18	8.34	-0.12	-0.86	0.16	0.04	0.01	0.00

n: sample size; SD: standard deviation; Min: minimum; Max: maximum; SE: standard error. Skewness: ideally 0 (for symmetry). A small amount of skew (between -1 and +1) is acceptable. Kurtosis: ideally 3 (for a normal distribution). Excess kurtosis of 0 is optimal.

The phenotypic data for Fusarium ear rot (FER) severity across 272 maize inbreds showed moderate disease levels and genetic variability. The overall FER score had a mean of 4.76 (on a 1–7 scale) with SD 1.58, and the distribution was approximately symmetric (skewness = –0.08, kurtosis = –0.92) (Table 1). Inoculated ears (mean 5.42) showed higher disease than naturally infected ears (mean 4.13).

Broad-sense heritability (H^2) without G×M was moderate for FER (0.61), Inoc (0.52), and NI (0.39), indicating a substantial genetic component in both modes. After incorporating the host-associated metagenome, H^2 increased by as much as 0.22 and was 0.83 (FER), 0.54 (Inoc), and 0.43 (NI). Across years for the combined scores (FER), the distribution was very similar (FER_2020: mean = 4.60, SD = 1.86; FER_2021: mean = 4.68, SD = 1.85). Broad-sense H^2 (no G×M) was 0.71 and 0.62 in 2020 and 2021, respectively; with G×M it was 0.71 and 0.75. By

trait and year, Inoc_2020 (mean = 5.24, SD = 2.10; skew = −0.38; kurt = −1.37; H^2 = 0.28, 0.31 with G×M) and Inoc_2021 (mean = 5.00, SD = 1.95; skew = −0.50; kurt = −1.02; H^2 = 0.50, 0.56 with G×M) both show negative skew, consistent with stress-testing that shifts more entries toward higher FER scores. NI_2020 (mean = 4.00, SD = 2.07; skew = 0.32; H^2 = 0.33, 0.36 with G×M) and NI_2021 (mean = 4.42, SD = 2.23; skew = −0.12; H^2 = 0.04, 0 with G×M) exhibit the widest variance, signaling stronger genotype×environment effects under natural epidemics specially in 2021.

The change from a right-skewed distribution in 2020 to a nearly balanced or slightly left-skewed one in 2021 matches the difference in field management. The 2020 plots were tilled, while the 2021 plots were not tilled. Tillage buries infected residue and lowers surface inoculum, whereas no-till keeps residue on the surface, changing the amount of fungal spores that influence disease spread. Along with year-to-year weather variation, these factors might explain why disease patterns and genotype performance differ between years. Altogether, the heritability results show that inoculated trials are effective for applying strong, uniform disease pressure and identifying the most susceptible lines early, while natural infection and overall FER composites, which maintain moderate to high heritability, are valuable for evaluating resistance under realistic field conditions.

Broad-sense heritability (H^2) reflected the overall repeatability of resistance across years, whereas narrow-sense heritability (h^2) captured the additive portion that determines genetic gain from selection. The increase in H^2 when the metagenome was included (H^2 [G×M]) indicates that genotype microbiome interactions explain part of the missing heritability and can improve the

reliability of resistance estimates. Using mixed models to combine data across years and management systems allows breeders to account for these genetic and microbial components, leading to more stable and accurate selection decisions.

The analysis of variance (ANOVA) for FER (Table 2) revealed significant effects of genotype (inbred line), treatment, and year on disease severity. Genotype had a highly significant effect on FER severity ($F = 2.57$, $p < 0.001$), showing substantial genetic variation among inbreds. Treatment was also highly significant ($F = 51.4$, $p < 0.001$), with artificial inoculation producing markedly higher disease scores than natural infection. Year effects were significant ($F = 11.91$, $p < 0.001$), indicating environmental differences between seasons, and a significant block effect ($F = 8.82$, $p = 0.003$) suggested some field heterogeneity. In contrast, the Treatment × Year interaction was not significant ($F = 2.90$, $p = 0.089$), implying that the inoculation effect was consistent across years.

Table 2. Analysis of variance (ANOVA) for Fusarium Ear Rot (FER) scores across inbreds, treatment (Inoc vs NI), year, and their interaction, with block effect; reported are df, sums of squares, mean squares, F values, and Pr(>F).

Source	Df	Sum Sq	Mean Sq	F Value	Pr(>F)
Inbred	272	2099.8	7.7	2.57	$<2e^{-16}$
Block	1	26.5	26.5	8.82	0.003
Treatment	1	154.8	154.8	51.4	$1.87E^{-12}$
Year	1	35.8	35.8	11.91	0.0006
Treatment × Year	1	8.7	8.7	2.90	0.089
Residuals	705	2121.6	3.0		

$p < 0.001$, $p < 0.01$, $p < 0.05$, $p < 0.1$.

Marker trait association

A total of 28 significant SNPs (representing 14 distinct loci) were identified for FER resistance, localized across six chromosomes (1, 2, 3, 6, 9, and 10). Some of the associated loci are supported by multiple SNPs above the statistical threshold. The largest number of signals mapped to chromosome 1 (6 unique SNPs in four chromosomal regions, followed by chromosomes 3 (5 unique SNPs in three chromosomal regions), chromosome 2 (3 unique SNPs in one chromosomal region), and two each on chromosomes 6, 9, and 10 (2 unique SNPs in 2 chromosomal regions) (Table 3).

The strongest associations ($-\log_{10}(p) \geq 6$) occurred on Chr 1 at 21.95 Mb, on Chr 10 at 141.89 Mb. A cluster of SNPs around 21.95 Mb on Chr 1 was found repeatedly in multiple traits and environments, yielding the highest $-\log_{10}(p)$ of 7.18 (NI) and 5–6 across traits like NI, FER, FER2021, and NI2020 scores in different years.

Several loci showed consistent detection across traits and environments. For example, the Chr 1 21.95 Mb region (near an AP2/EREBP TF) appeared in both FER and Natural infection (NI) data but not in the inoculated treatment, indicating an NI-driven, environment-specific effect that still registers in the combined FER trait. Similarly, SNPs on Chr 6 at 119.19 Mb were significant for both FER and NI, and SNPs on Chr 3 at 162.79 Mb (sucrose-phosphate synthase) were found in FER and inoculation datasets.

Table 3: Candidate genes identified through a genome-wide association study of Fusarium ear rot (FER) across inoculated and natural-infection trials in a maize diversity panel (B73 RefGen v4).

Trait	*SNP ID*	$-log_{10}(p)$			*Proximity (kb)*	*Ortholog and function*
		Add	*Dom Alt*	*Dom Ref*		
FER	1:9084925	3.6	0.27	**5.17**	*21.7*	RPM1 interacting protein 13 (RIN13) [1-C +]
NI	1:21953482	5.35	6.18	0.13	*16.9*	ereb236 AP2-EREBP-transcription factor 236 [1-C+]
FER	1:21953482	4.18	5.06	0.04	*16.9*	
NI	1:21953488	5.01	5.22	0.45	*16.9*	
NI	1:21953514	**7.18**	6.66	1.54	*16.9*	
FER2021	1:21953514	5.83	5.38	1.38		
FER	1:21953514	5.64	5.23	1.28		
NI 2020	1:21953514	5.08	4.65	1.33		
NI	1:254388616	**5.04**	5.04	NA	*1.9*	Ornithine cyclodeaminase/mu-crystallin family [2-NC]
Inoc2021	1:261020918	4.92	**5.41**	0.31	*Intronic*	FMP27-BLTP2_C_ [4-NC +]
FER	2:70649326	**5.98**	3.35	4.14	*52.5*	YSL6- yellow stripe-like transporter 6 [6-NC]
NI	2:70649502	5.15	5.8	0.7	*52. 7*	
FER	2:70649502	4.47	5.01	0.62		
Inoc2020	3:18760801	**5.21**	5.21	NA	*65.8*	Vitamin B6 photo-protection/homoeostasis (VB6) [2-NC +]

Table 3: Continued

Trait	*SNP ID*	$-log_{10}(p)$			*Proximity (kb)*	*Ortholog and function*
		Add	*Dom Alt*	*Dom Ref*		
FER2020	3:162757087	5.05	4.35	1.91	*98.1*	sucrose-phosphate synthase-like (sps2) v[3-NC+]
Inoc	3:162793006	**5.51**	5.51	NA	*62.2*	
Inoc	3:162793060	5.07	4.79	0.9	*62.1*	
FER2020	3:164307493	**5.61**	5.61	NA	*43.9*	Malic enzyme 15 [3-NC +]
NI 2020	3:164307493	5.55	5.55	NA	*43.9*	
FER	6:119197761	5.01	**5.41**	0.21	*26.5*	Phosphofructose kinase 1(PFK1) [3-NC +]
NI	6:119197761	4.8	5.24	0.3	*26.5*	
NI 2020	6:165760892	3.45	**5.49**	0.04	*24.8*	Triacylglycerol lipase 1[4-NC +]
FER2020	9:29728061	**5.39**	2.28	4.36	*31.1*	SNF1-related protein kinase (SnRK1) KIN11-like [3-NC +]
FER2020	9:49773560	5.1	5.64	0.46	*39451*	Phospholipid-transporting ATPase [4-NC]
NI 2020	9:49773560	4.87	**5.67**	0.2	*39451*	
NI	10:78829563	**5.47**	1.95	4.05	*5305*	Cytochrome P450 (CYP450) [5-C]
Inoc2020	10:141899030	**6.74**	6.42	1.34	*Intronic*	Villin-4 [7-C +]
Inoc	10:141899030	6.53	5.97	1.75		

Gene functions (C: canonical and NC: non-canonical): [1]Hormone and immune signaling, [2]Redox balance and stress protection, [3]Metabolic reprogramming, [4]Lipid metabolism and jasmonate precursors, [5]Defense compound biosynthesis and detoxification, [6]Metal homeostasis and micronutrient support, and [7]Cellular trafficking and defense organization, + LD-supported.

Key candidate genes reside at different loci (Table 3). On Chr 1, significant SNPs lie near Zm00001d027616, an RPM1-interacting protein 13 (RIP13/RIN13- family) homolog, and Zm00001d028069, an ereb236-AP2/ERF domain transcription factor 236. Other Chr 1 hits include an ornithine cyclodeaminase-crystallin family (Zm00001d033212) and an FMP27-(BLTP2) lipid-transfer protein (Zm00001d033375).

On Chr 2, the peak SNPs flank Zm00001d03941, a YSL6 metal-nicotianamine transporter. Chr 3 loci include a vitamin B_6 photoprotection and homeostasis biosynthesis protein (Zm00001d039903), Zm00001d042353 (a sucrose-phosphate synthase–like enzyme), and Zm00001d042392, a NADP-dependent me15-malic enzyme15. Chr 6 SNPs colocalize with Zm00001d037278 (phosphofructokinase1, PFK1) and Zm00001d038847 (triacylglycerol lipase 1). On Chr 9, we found a Zm00001d045633 SNF1-related kinase (SnRK1) (KIN11-like) and Zm00001d045956, a P-type phospholipid-transporting ATPase.

Finally, Chr 10 hits implicate Zm00001d024574 (a cytochrome P450) and Zm00001d026249 (villin-4 actin-binding protein). These genes span functions in signaling, defense, and redox metabolism, membrane structure, and carbon or lipid metabolism (Table 3).

Population Structure

Population structure of 272 inbred lines was assessed using principal component analysis (PCA), the genomic relationship matrix (GRM), a phylogenetic dendrogram, and sNMF ancestry proportions (Figure 3). The PCA scatterplot (Figure 3A) summarizes genome-wide relatedness. PC1 explains 20.5% of genomic variation and separates tropical/subtropical (TS) from temperate germplasm, whereas PC2 explains 10.1% and differentiates the temperate Stiff Stalk (SS) and

Non-Stiff Stalk (NSS) pools. Three clear clusters are evident, i.e., TS (blue), SS (red), and NSS (yellow), with numerous accessions occupying intermediate positions that reflect admixture (green). The strong horizontal separation indicates substantial divergence between tropical and temperate lineages, while the vertical spread captures within-temperate differentiation. The clear clusters, absence of distinct outliers, and smooth gradients indicate strong historical flow among groups, suggesting that the population structure can be adequately captured using only a few principal components.

The GRM heatmap (Figure 3B) illustrates pairwise genetic similarity among all maize inbreds based on genome-wide SNPs. Each pixel represents how closely related two lines are, where red indicates high similarity (shared ancestry) and green indicates low similarity (genetic distance). The main diagonal of bright red squares shows that each line is perfectly related to itself, and the large red blocks along this diagonal correspond to distinct genetic groups TS, SS, and NSS. Smaller sub-blocks within each major group indicate sets of closely related or near-duplicate lines that share recent pedigree segments. The dendrograms along the top and left edges cluster individuals with similar genomic profiles, showing that the panel is not genetically uniform but contains structured subpopulations. Green or dark regions between red blocks mark boundaries between divergent groups. For example, low relatedness between tropical and temperate lines or between two temperate heterotic pools, SS and NSS. The heatmap mirrors the population structure revealed by PCA/sNMF, showing strong within-group relatedness and lower between-group similarity. This visualization emphasizes the need to account for kinship in GWAS. Without modeling relatedness, shared ancestry can inflate false positives. Including the

GRM as a random effect (K matrix) corrects for these relationships, improves statistical accuracy, and helps identify closely related lines for data curation and balanced analysis design.

The circular dendrogram (Figure 3C) is a distance-based tree (Ward.D2) that organizes lines by genome-wide SNP similarity, providing a hierarchical view of how genotypes cluster. Branches separate three major clades corresponding to the tropical/subtropical (TS), Stiff Stalk (SS), and Non-Stiff Stalk (NSS) groups, with admixed lines appearing near branch junctions. Two clusters labeled Admixed (1) and Admixed (2) represent lines with mixed ancestry bridging the tropical and temperate clades, rather than distinct ancestral populations. Long branches between clades and short branches within clades indicate deep divergence among groups and closer relatedness within each group. The tree is useful for choosing diverse validation lines, planning crosses with strong heterotic contrast, and checking whether resistant entries occur across clades or are confined to one group.

The sNMF plot at K = 4 (Figure 3D) shows one vertical bar for each inbred, representing its proportional membership in four inferred ancestral components. Colors correspond to the main genetic groups like Stiff Stalk (SS, red), Non-Stiff Stalk (NSS, yellow), Tropical/Subtropical (TS, blue), with admixed lines (green) showing shared ancestry among them. Many lines display mixed membership, indicating continuous stratification and recent introgression among SS, NSS, and TS backgrounds. This plot shows both the number of ancestral components modeled (K) and how mixed each line is, and it agrees with the PCA and GRM results. Because structure is pronounced and graded rather than strictly discrete, downstream GWAS should include population covariates (e.g., top PCs) together with a

kinship/GRM term to control stratification and relatedness. The ancestry proportions also enable group-aware summaries (allele frequency/effect by background) and checks for enrichment of GWAS hits within specific lineages.

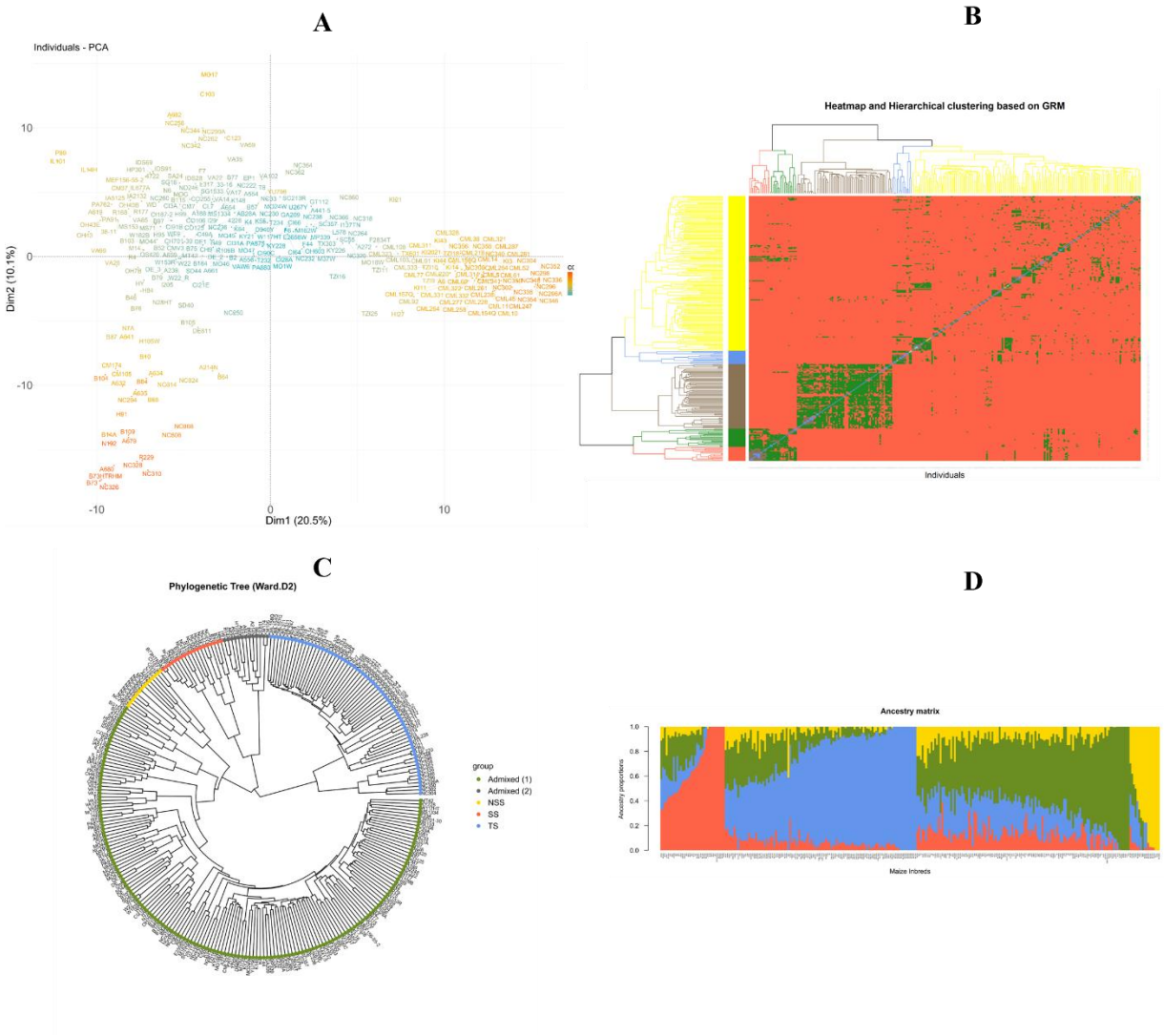

Figure 3. Population structure of 272 maize inbred lines. (A) Principal component analysis (PCA) of all inbreds, with each point colored by subgroup: tropical/subtropical (TS), stiff stalk (SS), non-stiff stalk (NSS), or admixed. **(B)** Heatmap of the genomic relationship matrix (GRM)

with hierarchical clustering. Relatedness blocks are evident along the diagonal, corresponding to TS, SS, and NSS subpopulations. **(C)** Circular phylogenetic dendrogram of the 272 lines based on genome-wide SNP distances. The dendrogram splits into three major clades corresponding to TS, SS, and NSS lineages. Admixed lines do not form a single clade but rather intermix between the major groups, appearing as branches between TS–SS or SS–NSS clades. **(D)** Ancestry coefficient matrix from sparse Non-negative Matrix Factorization (sNMF) at $K = 4$ ancestral populations. Each line is represented as a vertical bar partitioned into four colored segments that sum to 1. Panels A–D illustrate a structured yet admixed genetic architecture in this association panel, with clear separation of traditional maize subpopulations and moderate overlap among them.

Global LD analysis

Genome-wide LD decay with scatter or LOESS, genome-wide boxplots, and chromosome-wise boxplots show (Figure 4 A, B, C) that LD drops quickly with distance across the panel, where r^2 is highest for very close SNPs and then falls steadily. From the curves in our figures, r^2 is around 0.16–0.18 at very short distances, falls toward 0.10–0.12 within the next bins, and continues to decline. The median r^2 falls below 0.10 at 100 kb and is 0.05 by 300–500 kb. Chromosome-wise patterns are very similar, indicating fairly uniform mapping resolution across chromosomes. These results suggest using compact windows (±50–100 kb) for local LD inspection and candidate nomination and treating wider high-LD regions as multi-gene intervals.

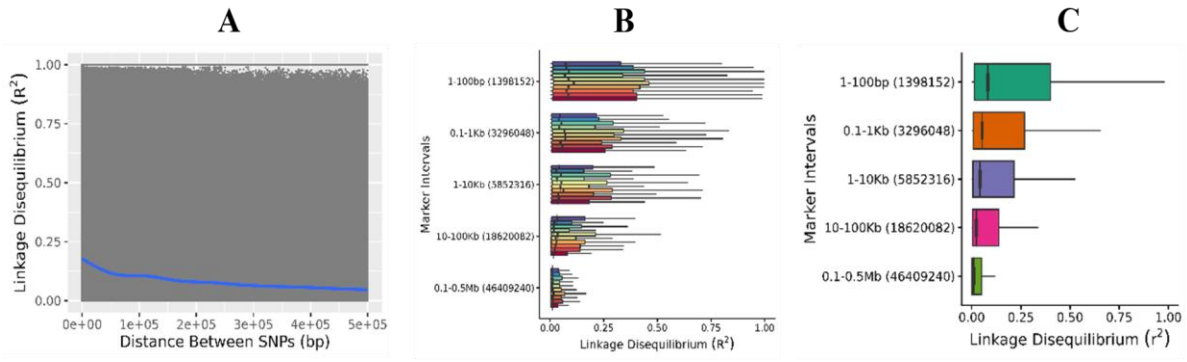

Figure 4 Global linkage disequilibrium (LD) in the study panel

(A) Genome-wide scatter of pairwise r^2 versus physical distance with a LOESS smooth (blue). **(B)** Chromosome-wise r^2 distributions are shown for five distance bins (1–100 bp, 0.1–1 kb, 1–10 kb, 10–100 kb, 0.1–0.5 Mb), labels include the number of SNP pairs per bin. **(C)** Genome-wide r^2 distributions for the same bins. Across the panel, LD drops rapidly with distance: r^2 is highest for adjacent SNPs (0.16–0.18), declines to 0.10–0.12, and continues to fall; the median r^2 drops below 0.10 by 100 kb and is 0.05 by 300–500 kb. Chromosome-wise patterns are similar, indicating broadly uniform mapping resolution.

Local LD analysis

Local LD patterns helped identify whether each significant SNP was linked to a single gene or a broader multi-gene region. On chromosome 1, the LD blocks at 9.08 Mb (RIN4) and 21.95 Mb (AP2/ERF-236) were compact and centered on the lead SNPs, indicating single-gene LD blocks, while the signal at 254.39 Mb (μ-crystallin/ornithine-cyclodeaminase-like) showed broader LD covering several nearby models and was treated as a multi-gene interval. Another region on Chr1 (261.02 Mb, FMP27/BLTP2) displayed a narrow LD cluster over a single gene. On chromosome 2 (70.65 Mb, YSL6), LD extended across multiple neighboring

genes, classifying it as a multi-gene interval. On chromosome 3, LD was confined to tight regions for VB6 (18.76 Mb), SPS2 (162.79 Mb), and NADP-ME (164.31 Mb), each forming single-gene LD blocks. Chromosome 6 showed similarly narrow LD for PFK1 (119.20 Mb) and Triacylglycerol lipase 1 (165.76 Mb), both single-gene blocks. On chromosome 9, SnRK1/KIN11 (29.73 Mb) had a small LD block limited to one gene, while P4-ATPase (49.77 Mb) covered a broader region with multiple genes. On chromosome 10, Villin-4 (141.90 Mb) exhibited a compact single-gene LD block, whereas Cytochrome P450 (78.83 Mb) showed a wider LD span involving more than one gene. Overall, ten loci (RIN4, AP2/ERF-236, FMP27/BLTP2, VB6, SPS2, NADP-ME, PFK1, TAG-lipase 1, SnRK1/KIN11, and Villin-4) were supported by tight single-gene LD blocks, while four regions (μ-crystallin/OCD-like, YSL6, P4-ATPase, and P450) showed broader LD and remain as multi-gene intervals pending fine-mapping or expression validation.

Discussion

Across the panel half of the loci, seven of fourteen appear in only one of the nine traits, indicating strong context specificity. Within a single year, overlaps are strongest between FER and natural infection, which share four of the fourteen loci and are much weaker between FER and inoculated disease, which share only one locus, and are totally absent between natural infection and inoculated disease, which share no loci at all. Only one of the fourteen loci, containing the AP2/ERF236 transcription factor, appears across both 2020 and 2021 within FER and natural infection. In total, four of the fourteen loci are associated with inoculated trials, including the one locus shared between FER and inoculated disease together with four loci that

are single-trait inoculated only. Hence, loci shared by FER and natural infection and those that repeat across years are prioritized as field-relevant, composite-influencing targets with the highest expected selection payoff, while inoculated-only hits remain informative but lower-ranking. The candidate genes at these loci include canonical direct-defense factors which are detected mainly in FER and natural infection, with Villin-4 providing a single inoculated-trial hit in 2020. Heritability rises when genotype-by-microbiome interactions are included in the models, indicating that a portion of the genetic control of FER resistance is only revealed when host loci are evaluated together with their associated microbiome.

Resistant inbreds (VA14, TZI10, SC55, NC320, MO45, H95, CML61, CML322, CML311, A635) stay at very low FER scores (0–2) in both years and in both inoculated and NI trials, showing that some lines carry durable, environment-stable resistance alleles. In contrast, the consistently high scores (5–7) of the susceptible group (SG1533, PA91, PA880, OH40B, NC314, NC312, NC268, M162W, F2834T, CMV3, CI28A, CI21E, B68, B52, B115, A634, A214N, 38-11) and the intermediate PA762, shows the quantitative, polygenic nature of FER and the presence of genotype-by-environment interaction in the panel.

Our field results address the long-recognized problem that FER resistance is highly environment-sensitive. Inoculated and natural infection imposes different disease pressures, and the FER composite mirrors natural epidemics best in our data while including metagenome terms recovers part of the missing heritability. PCA (Fig. 2A) is descriptive and shows clear separation by treatment (inoculated vs. NI) and by year. Evidence for genotype effects comes from the mixed models, which detected significant genotype terms. The distinct

orientation of Inoc_2020 and Inoc_2021 vectors relative to NI environments indicates that artificial inoculation created qualitatively different disease pressures from those under natural infection. This pattern is consistent with prior reports that FER resistance is environment-sensitive, with mode of infection and seasonal changes accounting for much of the phenotypic variation (Lanubile et al., 2017; Ayesiga et al., 2023). The large proportion of variance explained by PC1 and PC2 mainly reflects treatments (inoculated vs natural infection) and seasonal effects rather than discrete genetic clusters. Although PCA does not test significance, the clear year separation shows genotype and year contributions supports the need for multi-environment evaluation of quantitative disease traits.

The highest correlation between NI vs FER (0.90 overall and 0.89 in 2020) indicates that the combined FER index largely reflects performance under natural epidemics whereas only moderate correlation exists between Inoc vs NI (0.35 in 2021), suggesting partly distinct resistance mechanisms and environment management effects. Treatment difference between years 2020 tilled soil vs. 2021 no-till soil might have altered inoculum pressure. *Fusarium verticillioides* survive on corn residue but burying residue with tillage can reduce exposure of inoculum. Residue left on the surface in no-till can elevate local spore load, shaping natural infection dynamics and genotype rankings (Crop Protection Network-2024, UNL CropWatch, SDSU Extension). But published studies report mixed or inconsistent effects of tillage on ear-rot pathogens and mycotoxins across sites and seasons and weather frequently dominates realized risk.

Therefore, weather and insects often dominate realized risk. In field epidemics, ears are typically infected through the silk channel and occasionally through wounds, which helps explain why NI aligns most closely with FER. By contrast, artificial inoculation standardizes a high, uniform challenge (silk-channel or wound/needle), elevates means, and widens among-line differences while bypassing field bottlenecks, so genotype performance relationships can diverge across modes of infection (Lipps et al., 2025). Because fumonisin levels generally rise with FER severity, selecting NI/FER should also reduce toxin risk, although residue, weather, and genetic background can modulate toxin outcomes and should be verified with co-measured fumonisin assays (Lipps et al., 2025*)*. Therefore, programs should maintain parallel NI and inoculated trials, and analyze them jointly with multi-trait, multi-environment models to borrow information across models and years while capturing G×E.

The ridgeline densities show how disease imposition method and season shaped FER expression. Both years inoculated distributions were broader showing larger spread under uniform, forced exposure, whereas NI showed tighter, lower-mean profiles, especially in 2021 consistent with milder, more homogeneous field epidemics in that season. The pattern is expected because artificial inoculation standardizes inoculum and bypasses some field bottlenecks, while natural infection depends on silk exposure, weather at silking, and incidental wounding.

Thus, when natural pressure is low, scores cluster and discrimination among genotypes declines. The compact NI_2021 curve therefore shows that the epidemic was mild and the ratings were close together, which is common when disease severity is low and measured using

an ordinal scale (Chiang et al.,2022). Whereas, inoculated curves are broader because each ear receives a standardized silk-channel or wound inoculation, which raises means and increases spread. (Mesterhazy et al., 2020). NI will be highly dependent on silk timing and weather, whereas inoculation applies a uniform, high challenge. In years with light natural pressure, inoculation often improves discrimination among lines; conversely, NI can reveal field-relevant resistance tied to the natural silk-infection route that wound/needle tests may miss.

Year-to-year shifts in the NI curves reflect management and weather interactions rather than management alone. While residue retained under no-till can raise local inoculum and humidity, published studies report mixed or inconsistent effects of tillage on FER and fumonisin levels across sites and years (Herrera et al.,2023). In 2021, the smaller and more compact NI profile even under no-till likely relates to the weather conditions that year.

Insects can increase FER risk because feeding wounds open entry points for infection and are linked to higher ear rot and fumonisin levels (Parsons et al., 2010; Clements et al., 2003). In our trials, the fields were sprayed, and scouting showed little ear-feeding injury, so insect damage likely played only a minor role. The main difference we see between trials comes from how infection happens and how strong the disease pressure is. Natural infection (NI) depends on silk-channel infection under local weather and background inoculum, while inoculated trials apply a uniform, forced challenge through silk- or wound-type inoculation (Parsons et al., 2010). Because these two methods stress different parts of the plant's defense system, some genotypes behave similarly within the same type of test (for example, when we compare NI across years, or inoculated trials across years) but can behave differently when we compare NI to inoculation.

The ridge plots therefore suggest a two-step strategy: use inoculated trials first for strong early separation of lines, then confirm in NI/FER trials for field-relevant advancement. In production settings where ear feeding is a problem, managing insect wounding can further reduce FER risk and make phenotyping more consistent with on-farm conditions (Clements et al., 2003).

We used population-structure analysis (PCA, GRM, dendrogram, sNMF) to define our GWAS models and to interpret the biological relevance of FER-associated loci. All association tests were run as mixed models with top PCs and a genomic relationship matrix, and loci that did not remain under these corrections were treated as structure-driven and not advanced. For each lead SNP that passed this filter, we then examined subgroup allele frequencies and effect-size stability across SS, NSS, and TS, and re-fit models within groups and across environments (NI vs. inoculated). Signals that were consistent across backgrounds and environments were considered the strongest candidates for durable FER resistance.

Broad-sense heritability (H^2) was moderate to high for the composite traits and lower for single-year values, consistent with previous FER studies s (e.g., Lanubile et al., 2017; Orsi et al., 2025). These H^2 values indicate that a substantial portion of phenotypic variation is genetically determined, even though environmental variance remains large. The genotype term was significant in the mixed-model ANOVA, confirming heritable differences among lines, while strong treatment and year effects confirm the environmental influence. Narrow-sense heritability (h^2) for the combined traits was also high (for example, h^2 was 0.49 for FER, 0.39 for inoculated trials, and 0.29 for natural infection). This means that the additive genetic part should respond to selection in breeding. However, heritability values from a single year were less stable, which

suggests that the growing conditions in each year can change how resistance looks. In general, inoculated trials were more consistent than natural infection, because inoculation applies more uniform disease pressure. Natural infection showed more noise and more spread because it depends on weather and field conditions. Overall, this supports the need for repeated testing across years, and testing under both inoculated and natural infection, to get reliable breeding values for resistance.

Metagenome integration accounted for part of the missing heritability. H^2 increased from 0.61 to 0.83 for FER (an increase of 0.22), 0.52 to 0.54 for inoculated trials (an increase of 0.02), and 0.39 to 0.43 for natural infection (an increase of 0.04). This means that part of the variation in resistance, which could not be explained by genetics alone, is related to differences in the microbial communities linked to each plant. The effect of the metagenome was not the same in every case it was stronger in some years (such as FER in 2021) and smaller in others. This suggests that the microbiome interacts with the plant's genes in ways that depend on the environment. The benefit of including the metagenome is greatest when environmental conditions are more variable, while under controlled inoculated conditions, the improvement is smaller.

Candidate Genes and Pathways

Our phenotypic analysis and GWAS reveal that FER resistance in maize involves both typical defense genes and broader resistance pathways. Several of our candidate genes have clear roles in plant immunity. The RIP13/RIN13-family homolog near Zm00001d027616 is part of the RPM1-interacting protein family that serves as NLR-linked immune hubs. In Arabidopsis, RIN4

and RIN13 are distinct RPM1-interacting proteins with complementary roles in PTI/ETI signaling; maize also encodes homologs from this family. In *Arabidopsis*, RIN4 and RIN13 are distinct RPM1-interacting proteins with complementary roles in PTI/ETI signaling, and maize encodes homologs of this family. For example, Ray et al. (2019) reviews that RIN4 is a conserved immune regulator involved in the immune process through posttranslational modifications and plays roles in both PTI and ETI. Thus, our SNP near Zm00001d027616 (RPM1) suggests that nucleotide-binding leucine-rich repeat (NLR) signaling may contribute to FER resistance, possibly through recognition of *F. verticillioides* effectors.

Similarly, the AP2/EREBP-domain transcription factor (Zm00001d028069) at the Chr 1 locus likely coordinates hormone-mediated defense. AP2/ERF family proteins are well-known regulators of stress and defense genes, often integrating ethylene, jasmonate, and salicylic acid signals. For example, Su et al. (2025) demonstrate that AP2/ERF TFs typically activate the expression of downstream genes responsive to biotic stress through ET/JA/SA hormone pathways. Thus, Zm00001d028069 may promote expression of pathogenesis-related (PR) and other defense genes upon *Fusarium* challenge, fitting patterns in other pathosystems where ERF factors (like ZmERF061) enhance fungal resistance.

Our loci also implicate core metabolic and redox processes. The PFK1 gene (Zm00001d037278) on Chr 6 controls a rate-limiting step of glycolysis, likely supplying ATP and carbon skeletons needed for induced defenses. In general, sugar metabolism enzymes are often mobilized during defense with increased glycolysis fueling the oxidative burst and biosynthesis of defense compounds. Likewise, the sucrose-phosphate synthase like gene

(Zm00001d042353) on Chr 3 suggests enhanced sucrose production and carbon flux to support resistance. The malic enzyme (Zm00001d042392) (Figure 5) provides NADPH and pyruvate. NADPH is important for reactive-oxygen-species (ROS) detoxification and lignin/phenylpropanoid synthesis under pathogen attack. Previous work noted NADP-malic enzyme induction in defense (Sun et al., 2019). The vitamin B_6 enzyme (Zm00001d039903) (Figure 5) also helps control ROS accumulation. Together, these enzymes would supply energy and reduce NADPH required to fuel biosynthetic and detoxification reaction during defenses.

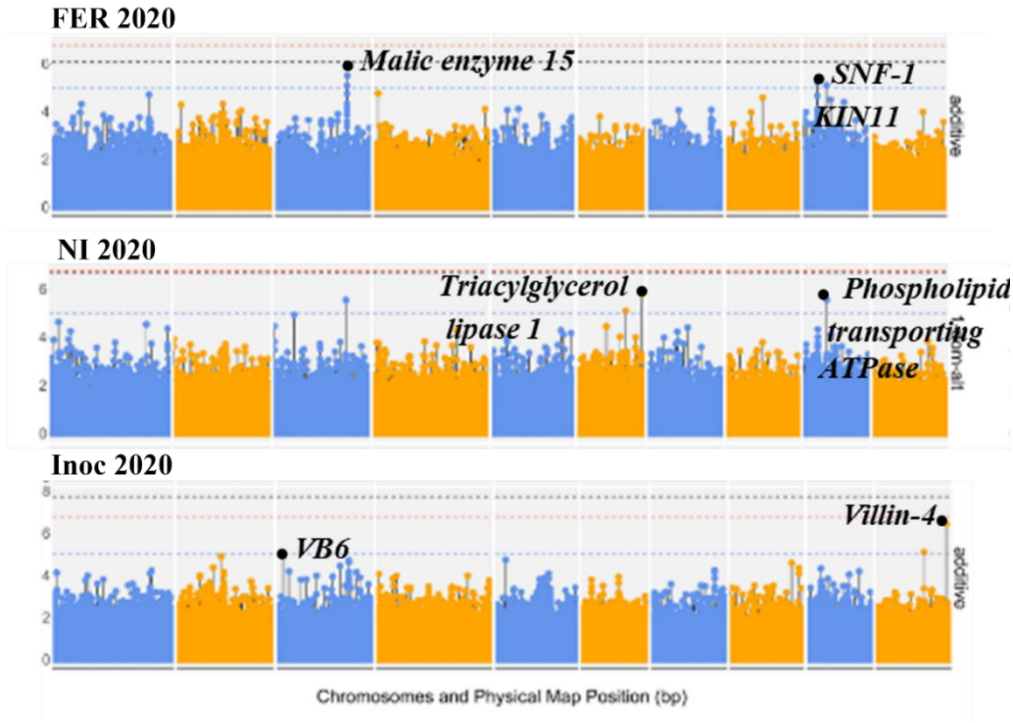

Figure 5 Manhattan plots display SNPs associations for FER resistance across three 2020 environments (FER_2020, NI_2020, Inoc_2020), with candidate genes annotated at significant loci, including Malic enzyme 15, SNF-1 related protein kinase (KIN11), Triacylglycerol lipase 1, Phospholipid-transporting ATPase, Vitamin B6, and Villin-4.

Functions like lipid metabolism and signaling genes also appear. A triacylglycerol lipase 1 (Zm00001d038847) (Figure 5) was detected that cleave fatty acids to generate oxylipin precursors. In maize, Zhu et al. (2022) showed that a triacylglycerol lipase (ZmTGL) activates salicylic-acid (SA) defenses against viral infection. By analogy, our lipase hit may release fatty acids for jasmonate synthesis or modulate membrane lipids during *Fusarium* infection (Xu et al., 2022). The FMP27-BLTP2 lipid-transfer protein (Zm00001d033375) (Figure 6) likely helps maintain membrane integrity during pathogen stress by shuttling lipids at membrane contact sites (Battilani et al., 2018). Also, the P4-type ATPase (Figure 5) on Chr 9 (Zm00001d045956) flips phospholipids to preserve membrane asymmetry. These membrane/lipid genes may contribute to controlling fungal penetration or mitigating toxin effects (Underwood et al., 2017). The cytochrome P450 (Zm00001d024574) on Chr 10 probably catalyzes synthesis of defense secondary metabolites (phytoalexins or detoxification products) (Irmisch et al., 2015). Finally, villin-4 (Zm00001d026249) (Figure 5) modulates the actin cytoskeleton; reorganized actin is known to be important for vesicle trafficking of defense cargo and for restricting pathogen spread (Henty-Ridilla et al., 2013).

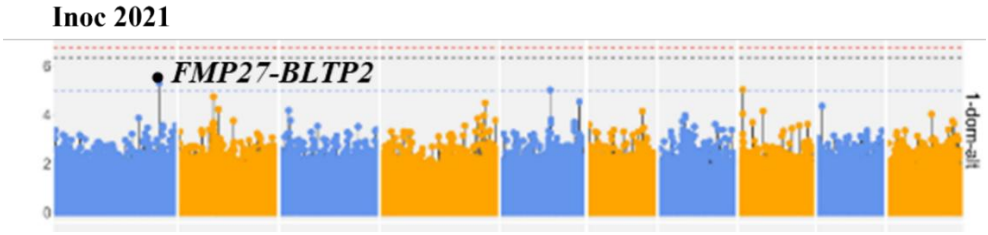

Figure 6 Manhattan plots display SNP associations for Fusarium Ear Rot (FER) resistance across 2021 environment (Inoc_2021), with candidate gene annotated at significant loci, including FMP27-BLTP2.

The identified SNF1-related kinase (SnRK1) (Zm00001d045633, KIN11-like) (Figure 5) connects metabolism to immune signaling. SnRK1 proteins sense cellular energy status and orchestrate defense–growth trade-offs. For example, Nietzsche et al. (2018) demonstrated in rice that overexpression of OsSnRK1a compromised growth but enhanced resistance to both biotrophic and necrotrophic pathogens, by boosting SA and priming JA pathways. Thus, our SnRK1 candidate likely acts as a master switch linking sugar starvation to defense activation. In maize and other plants, SnRK1 homologs have been reported to phosphorylate TFs or metabolic enzymes under stress, enhancing immune outputs.

Canonical Genes

The associations with FER resistance identified four canonical genes. A canonical gene in plants is a gene that encodes a component of well-established immune pathways and is supported by cross-species evidence for a direct role in biotic stress resistance (Li et al., 2020; Ding et al., 2022). RPM1-interacting protein 13(Figure 7) (RIN13-family homolog), a member of the RPM1-interacting protein family is a canonical gene that functions as an NLR-linked immune hub (Figure 7). In *Arabidopsis*, family members include RIN4 (a plasma-membrane guardee monitored by NLRs such as RPM1/RPS2) (Ray et al., 2019) and RIN13 (a nuclear interactor that can enhance RPM1-mediated resistance), Zm00001d027616 (RIN13-like; RPM1-interacting protein family),a maize homolog in the RIP13/RIN13 branch of the RPM1-interacting network supports a role for NLR-linked immune signaling. We therefore refer to this locus as RIN13-like (rather than ‘RIN4-like’) consistent with the maize annotation.

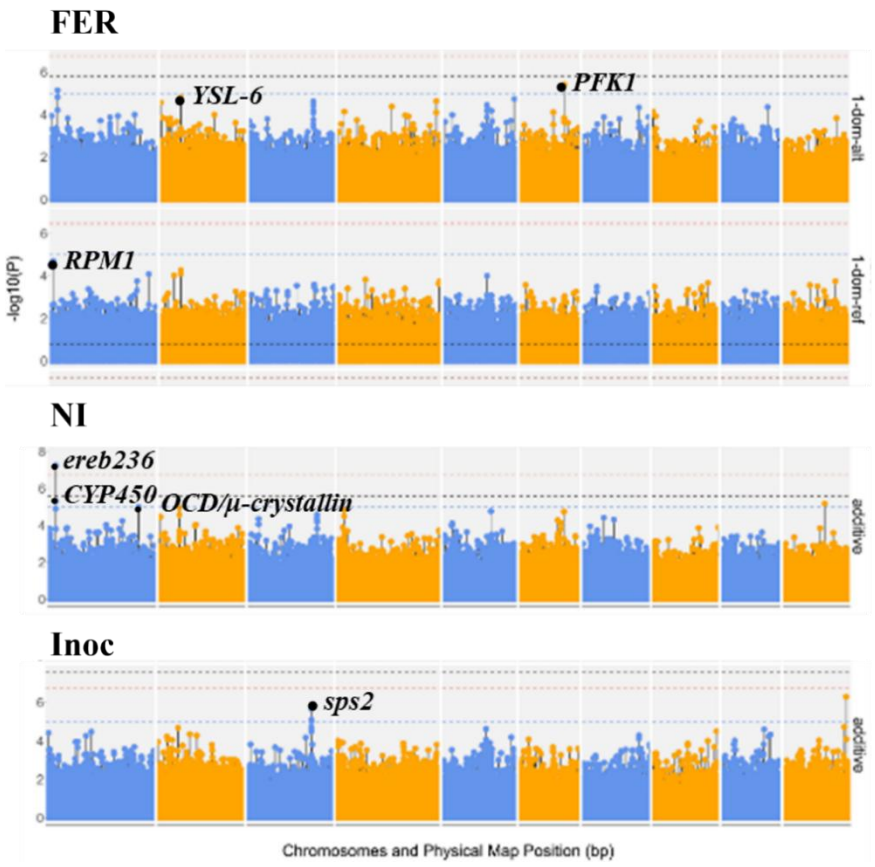

Figure 7 Manhattan plots display SNP associations for Fusarium Ear Rot (FER) resistance across three 2021 environments (FER_2021, NI_2021, Inoc_2021), with candidate genes annotated at significant loci, including RPM1 interacting protein 13 (RIP13), YSL6 (yellow stripe-like transporter 6), PFK1(Phosphofructose kinase 1), ereb236 (AP2-EREBP-transcription factor 236), CYP450 (Cytochrome P450), OCD/mu-crystallin family, and sucrose-phosphate synthase-like (sps2).

Likewise, The AP2/EREBP (APETALA2/ethylene-response factor) family (Figure 7) which is a large, plant-specific family of transcription factors provides responses to both abiotic and biotic stresses. For biotic stress, AP2/ERFs regulate downstream defense genes, are involved

in hormone signaling (SA, JA, ET) and are key components in disease resistance pathways and operate as master switches in defense gene expression (Ma et al., 2024). Cytochrome P450 (Figure 7) enzymes play important roles in the biosynthesis of defense-related secondary metabolites including phytoalexins, alkaloids, and flavonoids, as well as in the detoxification of pathogen-derived toxins and the modulation of hormone levels under infection, representing a canonical component of the chemical arm of plant immunity (Chakraborty et al., 2023). Villin-4, the final canonical gene, mediates cytoskeleton remodeling for plant immunity by regulating actin bundling and dynamics to coordinate vesicle trafficking of receptors and defense cargo and to reorganize actin at infection sites (Khurana et al., 2010).

Non-Canonical Genes

Beyond canonical hit, most signals point to auxiliary or non-canonical genes that support immunity indirectly through carbon and lipid metabolism, redox balance, and membrane lipid remodeling/transport. Multiple loci implicate energy or redox metabolism like PFK1 (Chr6) and SPS-like (Chr3:162.79 Mb) (Figure 7) which point to sugar-flux control that can feed immune outputs (Perby et al., 2022; Morkunas & Ratajczak, 2014), Likewise, NADP-malic enzyme (Zm00001d042392) and a vitamin-B6 enzyme (Zm00001d039903) (Figure3) support NADPH supply and ROS homeostasis during defense (Chen et al.,2019; Samsatly et al., 2016), while an ornithine cyclodeaminase or mu-crystallin family protein links amino acid and nitrogen metabolism to redox buffering, and the YSL6 metal–nicotianamine transporter (Figure 7) contributes to iron and micronutrient homeostasis that underpins ROS management and defense enzyme activity.

Membrane-lipid and trafficking nodes are represented by a triacylglycerol lipase-1 (Chr6) which is consistent with maize ZmTGL activating SA-mediated defenses and a P4-type phospholipid flippase (Chr9) and villin-4 (Chr10), which aligns with previous findings describing oxylipin/SA pathways and toxin or membrane detoxification through P4-ATPases, and actin-dependent trafficking of defense cargo (Xu et al., 2022; López-Marqués et al., 2023; Yang et al., 2022). FMP27/BLTP2_C (Zm00001d033375) is annotated as a Golgi-associated bridge-like lipid transfer protein (BLTP2/FMP27 family. BLTP2 proteins mediate bulk lipid transfer and organize membrane-contact sites, processes that can indirectly influence defense through membrane integrity, trafficking, and lipid signaling.

Finally, a SnRK1 (KIN11-like) kinase (Chr9) links energy status to defense trade-offs, a role widely noted for SnRK1-TOR circuitry under stress (Margalha et al., 2019). Therefore, our results recover four canonical genes at GWAS resolution replicate known FER modules at the pathway level (AP2/ERF signaling, P450/secondary metabolism, oxylipins, sugar-defense coupling), and introduce non-canonical gene-level candidates including SnRK1, PFK1, NADP-ME, VB6 enzyme, YSL6 transporter, P4-ATPase, triacylglycerol lipase, and SPS-like that expand the defense architecture underlying FER resistance while helping explain the environment-specific strength of the Chr 1:21.95 Mb signal under natural infection.

REFERENCES

Alamin, M., Sultana, M. H., Lou, X., Jin, W., & Xu, H. (2022). Dissecting complex traits using omics data: A review on the linear mixed models and their application in GWAS. *Plants*, *11*(23), 3277.

Alessandra, L., Luca, P., & Adriano, M. (2010). Differential gene expression in kernels and silks of maize lines with contrasting levels of ear rot resistance after *Fusarium* verticillioides infection. *Journal of plant physiology*, *167*(16), 1398-1406.

Amadeu, R. R., Garcia, A. A. F., Munoz, P. R., & Ferrão, L. F. V. (2023). AGHmatrix: genetic relationship matrices in R. *Bioinformatics*, *39*(7), btad445

Arata, A. F., Martínez, M., Castellari, C., Cristos, D., Pesquero, N. V., & Dinolfo, M. I. (2024). Impact of *Fusarium spp*. on different maize commercial hybrids: disease evaluation and mycotoxin contamination. *Fungal Biology*, *128*(6), 1983-1991.

Ayesiga, S. B., Rubaihayo, P., Oloka, B. M., Dramadri, I. O., & Sserumaga, J. P. (2024). Genome-wide association study and pathway analysis to decipher loci associated with Fusarium ear rot resistance in tropical maize germplasm. *Genetic Resources and Crop Evolution*, *71*(6), 2435-2448.

Basche, A. D., & DeLonge, M. S. (2019). Comparing infiltration rates in soils managed with conventional and alternative farming methods: A meta-analysis. *PloS one*, *14*(9), e0215702.

Battilani, P., Lanubile, A., Scala, V., Reverberi, M., Gregori, R., Falavigna, C., ... & Kolomiets, M. V. (2018). Oxylipins from both pathogen and host antagonize jasmonic acid-mediated

defence via the 9-lipoxygenase pathway in *Fusarium verticillioide*s infection of maize. *Molecular Plant Pathology*, *19*(9), 2162-2176.

Blandino, M., Saladini, M. A., Reyneri, A., Vanara, F., & Alma, A. (2008). The influence of sowing date and insecticide treatments on Ostrinia nubilalis (Hubner) damage and fumonisin contamination in maize kernels. *Maydica*, *53*(3), 199.

Blandino, M., Scarpino, V., Testa, G., Vanara, F., & Reyneri, A. (2022). The Effect of Foliar Fungicide and Insecticide Application on the Contamination of Fumonisins, Moniliformin and Deoxynivalenol in Maize Used for Food Purposes. *Toxins*, *14*(7), 42.

Bowen, K. L., & Hagan, A. K. TIMELY INFORMATION.

Bradbury, P. J., Zhang, Z., Kroon, D. E., Casstevens, T. M., Ramdoss, Y., & Buckler, E. S. (2007). TASSEL: software for association mapping of complex traits in diverse samples. *Bioinformatics*, *23*(19), 2633-2635.

Butoto, E. N., Marino, T. P., & Holland, J. B. (2021). Effects of artificial inoculation on trait correlations with resistance to Fusarium ear rot and fumonisin contamination in maize. *Crop Science*, *61*(4), 2522-2533.

Butoto, E. N., Brewer, J. C., & Holland, J. B. (2022). Empirical comparison of genomic and phenotypic selection for resistance to Fusarium ear rot and fumonisin contamination in maize. *Theoretical and Applied Genetics*, *135*(8), 2799-2816.

Bukowski, R., Guo, X., Lu, Y., Zou, C., He, B., Rong, Z., ... & Xu, Y. (2018). Construction of the third-generation Zea mays haplotype map. *Gigascience*, *7*(4), gix134.

Cao, A., de la Fuente, M., Gesteiro, N., Santiago, R., Malvar, R. A., & Butrón, A. (2022). Genomics and pathways involved in maize resistance to Fusarium ear rot and kernel contamination with fumonisins. *Frontiers in plant science*, *13*, 866478.

Cavaglieri, L. R., Passone, A., & Etcheverry, M. G. (2004). Correlation between screening procedures to select root endophytes for biological control *of Fusarium verticillioides* in Zea mays L. *Biological Control*, *31*(3), 259-267.

Chakraborty, P., Biswas, A., Dey, S., Bhattacharjee, T., & Chakrabarty, S. (2023). Cytochrome P450 gene families: role in plant secondary metabolites production and plant defense. *Journal of Xenobiotics*, *13*(3), 402-423.

Chen, Q., Wang, B., Ding, H., Zhang, J., & Li, S. (2019). The role of NADP-malic enzyme in plants under stress. *Plant science*, *281*, 206-212.

Chiang, K. S., & Bock, C. H. (2022). Understanding the ramifications of quantitative ordinal scales on accuracy of estimates of disease severity and data analysis in plant pathology. *Tropical plant pathology*, *47*(1), 58-73.

Clements, M. J., Kleinschmidt, C. E., Maragos, C. M., Pataky, J. K., & White, D. G. (2003). Evaluation of inoculation techniques for Fusarium ear rot and fumonisin contamination of corn. Plant Disease, 87(2), 147-153.

Crop Protection Network. (2024, December 11). *An overview of Ear rots.*

Crop Protection Network. (2024, March 12). *Corn disease loss estimates from the United States and Ontario, Canada — 2023*. https://cropprotectionnetwork.org/publications/corn-disease-loss-estimates-from-the-united-states-and-ontario-canada-2023

Czembor, E., Stępień, Ł., & Waśkiewicz, A. (2015). Effect of environmental factors on *Fusarium* species and associated mycotoxins in maize grain grown in Poland. *PloS one*, *10*(7), e0133644

Devlin, B., & Roeder, K. (1999). Genomic control for association studies. *Biometrics*, *55*(4), 997-1004.

Ding, L. N., Li, Y. T., Wu, Y. Z., Li, T., Geng, R., Cao, J., ... & Tan, X. L. (2022). Plant disease resistance-related signaling pathways: recent progress and future prospects. *International Journal of Molecular Sciences*, *23*(24), 16200.

Dragich, M., & Nelson, S. (2014). Gibberella and Fusarium ear rots of maize in Hawai ‘i. Plant Disease, 102, 1-8.

Du, S., & Xiong, W. (2024). Weather Extremes Shock Maize Production: Current Approaches and Future Research Directions in Africa. Plants, 13(12), 1585.

Eichenseer, H., Strohbehn, R., & Burks, J. C. (2014). Frequency and severity of western bean cutworm (Lepidoptera: Noctuidae) ear damage in transgenic corn hybrids expressing different Bacillus thuringiensis cry toxins. Journal of Economic Entomology, 101(2), 555-563.

Erenstein, O., Jaleta, M., Sonder, K., Mottaleb, K., & Prasanna, B. M. (2022). Global maize production, consumption, and trade: trends and R&D implications. *Food security*, *14*(5), 1295-1319.

Finkina, E. I., Melnikova, D. N., & Bogdanov, I. V. (2016). Lipid transfer proteins as components of the plant innate immune system: structure, functions, and applications. *Acta Naturae (англоязычная версия)*, *8*(2 (29)), 47-61.

Flett, B. C., McLaren, N. W., & Wehner, F. C. (1998). Incidence of ear rot pathogens under alternating corn tillage practices. *Plant Disease*, *82*(7), 781-784.

Flint-Garcia, S. A., Thuillet, A. C., Yu, J., Pressoir, G., Romero, S. M., Mitchell, S. E., ... & Buckler, E. S. (2005). Maize association population: a high-resolution platform for quantitative trait locus dissection. *The plant journal*, *44*(6), 1054-1064.

Forni, S., Aguilar, I., & Misztal, I. (2011). Different genomic relationship matrices for single-step analysis using phenotypic, pedigree and genomic information. *Genetics Selection Evolution*, *43*(1), 1.

G. (2003). Evaluation of inoculation techniques for Fusarium ear rot and fumonisin contamination of corn. *Plant Disease*, *87*(2), 147-153.

Gaikpa, D. S., & Miedaner, T. (2019). Genomics-assisted breeding for ear rot resistances and reduced mycotoxin contamination in maize: methods, advances, and prospects. *Theoretical and Applied Genetics*, *132*, 2721-2739.

Gianola, D., Fariello, M. I., Naya, H., & Schön, C. C. (2016). Genome-wide association studies with a genomic relationship matrix: a case study with wheat and Arabidopsis. *G3: Genes, Genomes, Genetics*, *6*(10), 3241-3256.

Gamanya, R., & Sibanda, L. (2001). Survey of *Fusarium moniliforme (F. verticillioides)* and production of fumonisin B1 in cereal grains and oilseeds in Zimbabwe. *International journal of food microbiology*, *71*(2-3), 145-149.

Gianola, D., Fariello, M. I., Naya, H., & Schön, C. C. (2016). Genome-wide association studies with a genomic relationship matrix: a case study with wheat and Arabidopsis. *G3: Genes, Genomes, Genetics*, *6*(10), 3241-3256.

Hudson, O., Meinecke, C. D., & Brawner, J. T. (2024). Comparative genomics of *Fusarium* species causing *Fusarium* ear rot of maize. *PloS one*, *19*(10), e0306144.

Henty-Ridilla, J. L., Shimono, M., Li, J., Chang, J. H., Day, B., & Staiger, C. J. (2013). The plant actin cytoskeleton responds to signals from microbe-associated molecular patterns. *PLoS pathogens*, *9*(4), e1003290.

Herrera, M., Cavero, J., Franco-Luesma, S., Álvaro-Fuentes, J., Ariño, A., & Lorán, S. (2023). Mycotoxins and crop yield in maize as affected by irrigation management and tillage practices. *Agronomy*, *13*(3), 798.

Irmisch, S., Zeltner, P., Handrick, V., Gershenzon, J., & Köllner, T. G. (2015). The maize cytochrome P450 CYP79A61 produces phenylacetaldoxime and indole-3-acetaldoxime in heterologous systems and might contribute to plant defense and auxin formation. *BMC Plant Biology*, *15*(1), 128.

Jambhulkar, P. P., Bajpai, R., Reddy, H. J., Tripathy, P. S., Varun, P., Rout, A. K., ... & Nanjundappa, M. (2024). Assessment of Genetic Diversity and the Population Structure

of Species from the *Fusarium fujikuroi* Species Complex Causing Fusarium Stalk Rot of Maize. *Journal of Fungi*, *10*(8), 574.

Janse van Rensburg, B. J., Mc Laren, N. W., Schoeman, A., & Flett, B. C. (2016). The effects of cultivar and prophylactic fungicide spray for leaf diseases on colonization of maize ears by fumonisin producing *Fusarium* spp. and fumonisin synthesis in South Africa. *Crop Protection*, *79*, 56-63. Structure of Species from the *Fusarium fujikuroi* Species Complex Causing Fusarium Stalk Rot of Maize. *Journal of Fungi*, *10*(8), 574.

Kang, H. M., Sul, J. H., Service, S. K., Zaitlen, N. A., Kong, S. Y., Freimer, N. B., ... & Eskin, E. (2010). Variance component model to account for sample structure in genome-wide association studies. *Nature genetics*, *42*(4), 348-354.

Khurana, P., Henty, J. L., Huang, S., Staiger, A. M., Blanchoin, L., & Staiger, C. J. (2010). Arabidopsis VILLIN1 and VILLIN3 have overlapping and distinct activities in actin bundle formation and turnover. *The Plant Cell*, *22*(8), 2727-2748.

Korte, A., and Farlow, A. (2013). The advantages and limitations of trait analysis with GWAS: a review. Plant Methods 9:29. doi: 10.1186/1746- 4811-9-29

Lanubile, A., Maschietto, V., Borrelli, V. M., Stagnati, L., Logrieco, A. F., & Marocco, A. (2017). Molecular basis of resistance to Fusarium ear rot in maize. *Frontiers in plant science*, *8*, 1774.

Licht, M., & Archontoulis, S. (2017). Influence of drought on corn and soybean.

Lipka, A. E., Tian, F., Wang, Q., Peiffer, J., Li, M., Bradbury, P. J., ... & Zhang, Z. (2012). GAPIT: genome association and prediction integrated tool. *Bioinformatics*, *28*(18), 2397-2399.

Lee, H. J., & Ryu, D. (2015). Advances in mycotoxin research: public health perspectives. *Journal of food science*, *80*(12), T2970-T2983.

Li, L., Jiang, F., Bi, Y., Yin, X., Zhang, Y., Li, S., ... & Fan, X. (2024). Dissection of Common Rust Resistance in Tropical Maize Multiparent Population through GWAS and Linkage Studies. *Plants*, *13*(10), 1410.

Li, P., Lu, Y. J., Chen, H., & Day, B. (2020). The lifecycle of the plant immune system. *Critical reviews in plant sciences*, *39*(1), 72-100.

Lipps, S., Sorensen, P., Krone, M., Mideros, S., & Jamann, T. (2025). Inoculation of maize ears with *Fusarium graminearum* to study Gibberella ear rot. *Cold Spring Harbor Protocols*.

Lipps, S., Bohn, M., Rutkoski, J., Butts-Wilmsmeyer, C., Mideros, S., & Jamann, T. (2025). Comparative review of *Fusarium graminearum* infection in maize and wheat: Similarities in resistance mechanisms and future directions. *Molecular Plant-Microbe Interactions*, *38*(2), 142-159.

López-Marqués, R. L. (2023). Mini-review: Lipid flippases as putative targets for biotechnological crop improvement. *Frontiers in Plant Science*, *14*, 1107142.

Ma, N., Sun, P., Li, Z. Y., Zhang, F. J., Wang, X. F., You, C. X., ... & Zhang, Z. (2024). Plant disease resistance outputs regulated by AP2/ERF transcription factor family. *Stress Biology*, *4*(1), 2.

Ma, Z., Wang, W., Chen, X., Gehman, K., Yang, H., & Yang, Y. (2024). Prediction of the global occurrence of maize diseases and estimation of yield loss under climate change. *Pest Management Science*.

Margalha, L., Confraria, A., & Baena-González, E. (2019). SnRK1 and TOR: modulating growth–defense trade-offs in plant stress responses. *Journal of experimental botany*, *70*(8), 2261-2274.

Masiello, M., Somma, S., Ghionna, V., Logrieco, A. F., & Moretti, A. (2019). In vitro and in-field response of different fungicides against Aspergillus flavus and Fusarium species causing ear rot disease of maize. *Toxins*, *11*(1), 11.

Maschietto, V., Lanubile, A., De Leonardis, S., Marocco, A., & Paciolla, C. (2016). Constitutive expression of pathogenesis-related proteins and antioxydant enzyme activities triggers maize resistance towards *Fusarium verticillioides*. *Journal of Plant Physiology*, *200*, 53-61.

Mesterházy, Á., Lemmens, M., & Reid, L. M. (2012). Breeding for resistance to ear rots caused by *Fusarium* spp. in maize–a review. *Plant breeding*, *131*(1), 1-19.

Mesterhazy, A., Szieberth, D., Toldine, E. T., Nagy, Z., Szabó, B., Herczig, B., ... & Tóth, B. (2022). Updating the methodology of identifying maize hybrids resistant to ear rot pathogens and their toxins—Artificial inoculation tests for kernel resistance to *Fusarium graminearum*, F. verticillioides, *and Aspergillus flavus*. *Journal of Fungi*, *8*(3), 293.

Mesterhazy, A., Toldine Toth, E., Szel, S., Varga, M., & Toth, B. (2020). Resistance of maize hybrids *to Fusarium graminearum, F. culmorum, and F. verticillioides* ear rots with

toothpick and silk channel inoculation, as well as their toxin production. *Agronomy*, *10*(9), 1283.

Morkunas, I., & Ratajczak, L. (2014). The role of sugar signaling in plant defense responses against fungal pathogens. *Acta Physiologiae Plantarum*, *36*(7), 1607-1619.

Munkvold, G. P. (2003). Cultural and genetic approaches to managing mycotoxins in maize. *Annual review of phytopathology*, *41*(1), 99-116.

Munkvold, G.P. Cultural and genetic approaches to managing mycotoxins in maize. *Annu. Rev. Phytopathol.* 2003, *41*, 99–116.

Parsons, M. W., & Munkvold, G. P. (2010). Associations of planting date, drought stress, and insects with Fusarium ear rot and fumonisin B1 contamination in California maize. *Food Additives and Contaminants*, *27*(5), 591-607.

Pearson, T. A., & Manolio, T. A. (2008). How to interpret a genome-wide association study. *Jama*, *299*(11), 1335-1344.

Peiffer, J. A., Spor, A., Koren, O., Jin, Z., Tringe, S. G., Dangl, J. L., ... & Ley, R. E. (2013). Diversity and heritability of the maize rhizosphere microbiome under field conditions. *Proceedings of the National Academy of Sciences*, *110*(16), 6548-6553.

Perby, L. K., Richter, S., Weber, K., Hieber, A. J., Hess, N., Crocoll, C., ... & Mustroph, A. (2022). Cytosolic phosphofructokinases are important for sugar homeostasis in leaves of Arabidopsis thaliana. *Annals of Botany*, *129*(1), 37-52.

Perochon, A., & Doohan, F. M. (2024). Trichothecenes and fumonisins: Key players in Fusarium–cereal ecosystem interactions. *Toxins*, *16*(2), 90.

Rajath, H. P., Kumar, C., Hanumanthappa, M., Bhanuprakash, H. R., Yogesh, G. S., & Chandrakala, H. (2023). Impact of weather parameters on maize agroecosystem and adaptation strategies under changing climatic conditions: A review: Sustainable and climate-resilient adaptation strategies in maize agroecosystem. *Plant Science Today*, *10*(sp1), 01-10.

Ray, S. K., Macoy, D. M., Kim, W. Y., Lee, S. Y., & Kim, M. G. (2019). Role of RIN4 in regulating PAMP-triggered immunity and effector-triggered immunity: current status and future perspectives. *Molecules and Cells*, *42*(7), 503-511.

Rosyara, U. R., De Jong, W. S., Douches, D. S., & Endelman, J. B. (2016). Software for genome-wide association studies in autopolyploids and its application to potato. *The plant genome*, *9*(2), plantgenome2015-08.

Samsatly, J., Chamoun, R., Gluck-Thaler, E., & Jabaji, S. (2016). Genes of the de novo and Salvage Biosynthesis Pathways of Vitamin B6 are Regulated under Oxidative Stress in the Plant Pathogen Rhizoctonia solani. *Frontiers in microbiology*, *6*, 1429.

Schmidt, P., Hartung, J., Bennewitz, J., & Piepho, H. P. (2019). Heritability in plant breeding on a genotype-difference basis. *Genetics*, *212*(4), 991-1008.

SDSU Extension. (2022, February 10). *Gibberella and Fusarium ear rots developing in corn*.

Segura, V., Vilhjálmsson, B. J., Platt, A., Korte, A., Seren, Ü., Long, Q., & Nordborg, M. (2012). An efficient multi-locus mixed-model approach for genome-wide association studies in structured populations. *Nature genetics*, *44*(7), 825-830.

Solórzano-Solórzano, J. A., Zambrano, S. M. V., & Olmedo, J. B. V. (2024). *Fusarium spp.* en el cultivo de maíz: Identificación, distribución geográfica, sintomatología, micotoxinas, ciclo de la enfermedad, control, y desafíos actuales y futuros. *Scientia Agropecuaria*, *15*(4), 537-556.

Skoglund, L. G., & Brown, W. M. (1988). Effects of tillage regimes and herbicides on *Fusarium* species associated with corn stalk rot. *Canadian Journal of Plant Pathology*, *10*(4), 332-338.

Stagnati, L., Lanubile, A., Samayoa, L. F., Bragalanti, M., Giorni, P., Busconi, M., ... & Marocco, A. (2019). A genome wide association study reveals markers and genes associated with resistance to *Fusarium verticillioides* infection of seedlings in a maize diversity panel. *G3: Genes, Genomes, Genetics*, *9*(2), 571-579.

Sun, X., Han, G., Meng, Z., Lin, L., & Sui, N. (2019). Roles of malic enzymes in plant development and stress responses. *Plant signaling & behavior*, *14*(10), e1644596.

Syngenta Crop Protection LLC. (2023). *Miravis® Neo fungicide-U.S. label* (PDF). Retrieved from Greenbook. https://assets.greenbook.net/20-05-21-29-08-2023-Miravis_Neo_-_label.pdf

Thakur, Kajal, Neha Salaria, Baljeet Singh, Vinay Bhardwaj, Sarvjeet Kukreja, and Umesh Goutam. "Unravelling the potential of susceptibility genes in plant disease management: Present status and future prospects." *Plant science today* 10, no. sp1 (2023): 46-55

Underwood, W., Ryan, A., & Somerville, S. C. (2017). An Arabidopsis lipid flippase is required for timely recruitment of defenses to the host–pathogen interface at the plant cell surface. *Molecular Plant*, *10*(6), 805-820.

UNL CropWatch. (2017, September 29). *Ear rot diseases developing in some Nebraska corn fields*

U.S. Department of Agriculture, Foreign Agricultural Service. (2024). *Corn: U.S. corn exports in 2024*. U.S. Department of Agriculture.

U.S. Department of Agriculture, National Agricultural Statistics Service. (2025, January 10). *Corn production down, soybean production up in 2024, USDA reports* [News release].

U.S. Department of Agriculture, National Agricultural Statistics Service. (2025a, January 10). *Crop production 2024 summary*. U.S. Department of Agriculture.

U.S. Environmental Protection Agency. (2015). *Proline® 480 SC (prothioconazole) pesticide product label* (EPA Reg. No. 264-825).

VanRaden, P. M. (2008). Efficient methods to compute genomic predictions. *Journal of dairy science*, *91*(11), 4414-4423.

Vitezica, Z. G., Varona, L., & Legarra, A. (2013). On the additive and dominant variance and covariance of individuals within the genomic selection scope. *Genetics*, *195*(4), 1223-1230.

Wagner, M. R. (2022). How hungry roots get their microbes. *Elife*, *11*, e82391.https://www3.epa.gov/pesticides/chem_search/ppls/000264-00825-20150210.pdf

Wallace, J. G., Bradbury, P. J., Zhang, N., Gibon, Y., Stitt, M., & Buckler, E. S. (2014). Association mapping across numerous traits reveals patterns of functional variation in maize. *PLoS genetics*, *10*(12), e1004845.

Walters, W. A., Jin, Z., Youngblut, N., Wallace, J. G., Sutter, J., Zhang, W., ... & Ley, R. E. (2018). Large-scale replicated field study of maize rhizosphere identifies heritable microbes. *Proceedings of the National Academy of Sciences*, *115*(28), 7368-7373.

Wang, H., Chang, T. S., Dombroski, B. A., Cheng, P. L., Patil, V., Valiente-Banuet, L., ... & Lee, W. P. (2024). Whole-genome sequencing analysis reveals new susceptibility loci and structural variants associated with progressive supranuclear palsy. *Molecular neurodegeneration*, *19*(1), 61.

Wang, J., & Zhang, Z. (2021). GAPIT version 3: boosting power and accuracy for genomic association and prediction. *Genomics, proteomics & bioinformatics*, *19*(4), 629-640.

Wientjes, Y. C., Bijma, P., Vandenplas, J., & Calus, M. P. (2017). Multi-population genomic relationships for estimating current genetic variances within and genetic correlations between populations. *Genetics*, *207*(2), 503-515.

Wu, D., Tanaka, R., Li, X., Ramstein, G. P., Cu, S., Hamilton, J. P., ... & Gore, M. A. (2021). High-resolution genome-wide association study pinpoints metal transporter and chelator genes involved in the genetic control of element levels in maize grain. *G3*, *11*(4), jkab059.

Xu, X. J., Geng, C., Jiang, S. Y., Zhu, Q., Yan, Z. Y., Tian, Y. P., & Li, X. D. (2022). A maize triacylglycerol lipase inhibits sugarcane mosaic virus infection. *Plant Physiology*, *189*(2), 754-771.

Yan, J., Shah, T., Warburton, M. L., Buckler, E. S., McMullen, M. D., & Crouch, J. (2009). Genetic characterization and linkage disequilibrium estimation of a global maize collection using SNP markers. *PloS one*, *4*(12), e8451.

Yang, Y., Niu, Y., Chen, T., Zhang, H., Zhang, J., Qian, D., ... & Xiang, Y. (2022). The phospholipid flippase ALA3 regulates pollen tube growth and guidance in Arabidopsis. *The Plant Cell*, *34*(10), 3718-3736.

Yang, Z., Zhao, T., Cheng, H., & Yang, J. (2024). Microbiome-enabled genomic selection improves prediction accuracy for nitrogen-related traits in maize. *G3: Genes, Genomes, Genetics*, *14*(3), jkad286.

Yao, L., Li, Y., Ma, C., Tong, L., Du, F., & Xu, M. (2020). Combined genome-wide association study and transcriptome analysis reveal candidate genes for resistance to Fusarium ear rot in maize. *Journal of integrative plant biology*, *62*(10), 1535-1551.

Yu, J., Pressoir, G., Briggs, W. H., Vroh Bi, I., Yamasaki, M., Doebley, J. F., ... & Buckler, E. S. (2006). A unified mixed-model method for association mapping that accounts for multiple levels of relatedness. *Nature genetics*, *38*(2), 203-208.

Zhang, Z., Ersoz, E., Lai, C. Q., Todhunter, R. J., Tiwari, H. K., Gore, M. A., ... & Buckler, E. S. (2010). Mixed linear model approach adapted for genome-wide association studies. *Nature genetics*, *42*(4), 355-360.

Zila, C. T., Ogut, F., Romay, M. C., Gardner, C. A., Buckler, E. S., & Holland, J. B. (2014). Genome-wide association study of Fusarium ear rot disease in the USA maize inbred line collection. *BMC plant biology*, *14*(1), 372.

Zuffo, L. T., DeLima, R. O., & Lübberstedt, T. (2022). Combining datasets for maize root seedling traits increases the power of GWAS and genomic prediction accuracies. *Journal of Experimental Botany*, *73*(16), 5460-5473.

APPENDIX

Supplemental Figures

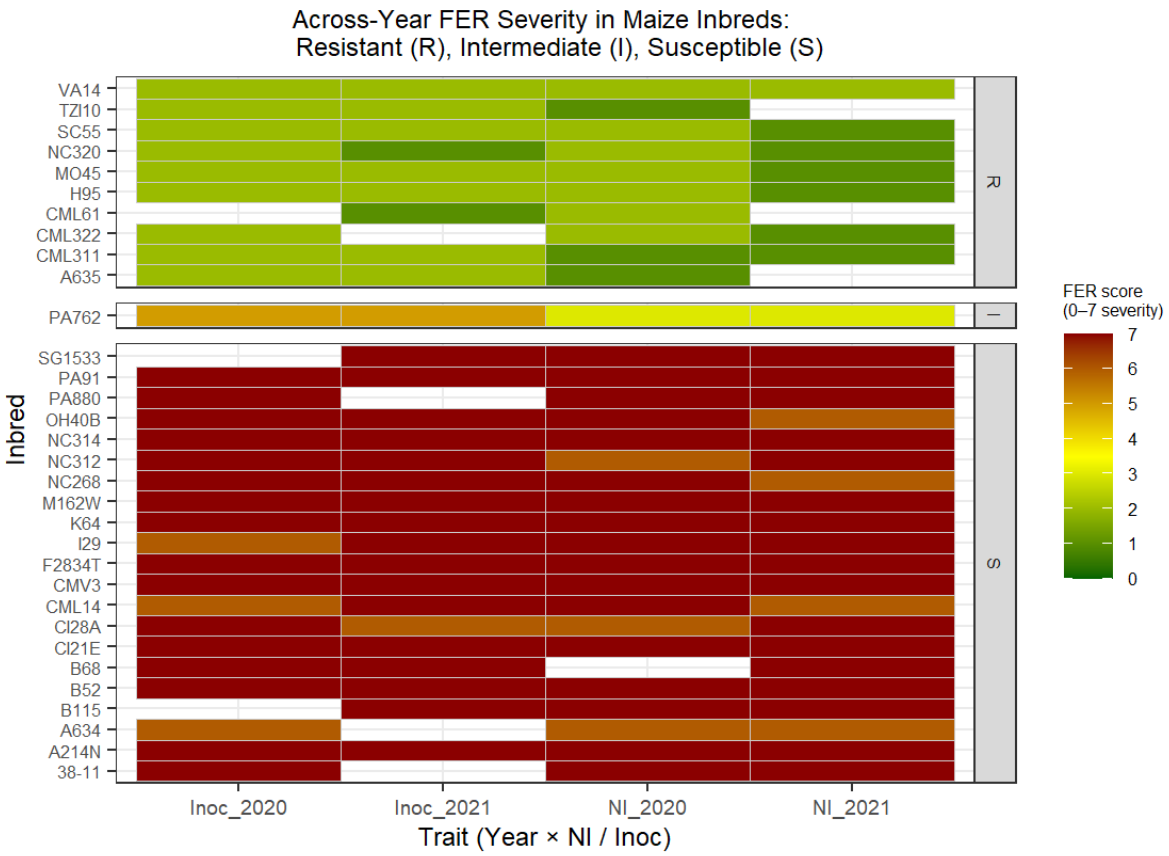

Figure S1: **Heatmap showing FER severity scores (0–7 scale) for each inbred line evaluated across two years (2020, 2021) and two disease environments: inoculated (Inoc_2020, Inoc_2021) and natural infection (NI_2020, NI_2021).** Inbreds are grouped into Resistant (R), Intermediate (I), and Susceptible (S) categories based on their consistent across-year performance. Color gradients depict increasing disease severity from green (low FER) to red (high FER)

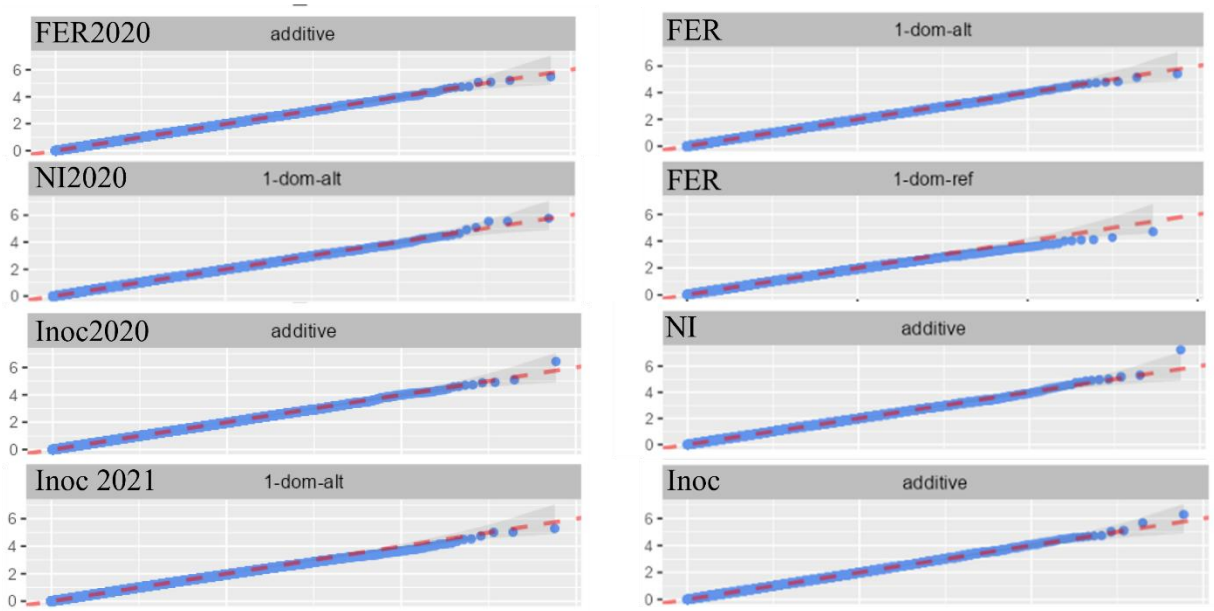

Figure S2 Quantile–quantile (Q–Q) plots. Observed $-\log_{10}(p)$ (x-axis) values are shown for multiple FER-related traits (FER2020, NI2020, Inoc2020, Inoc2021, FER, NI, Inoc) using the best-fitting model among three genotype-effect models: additive, dominant-alternative (1-dom-alt), and dominant-reference (1-dom-ref). The red dashed line represents the null expectation under no marker–trait association. The blue points represent the observed test statistics, which deviate from the red diagonal at the far-right tail, indicating true association signals demonstrating good overall model performance and effective control of false-positive associations across environments.

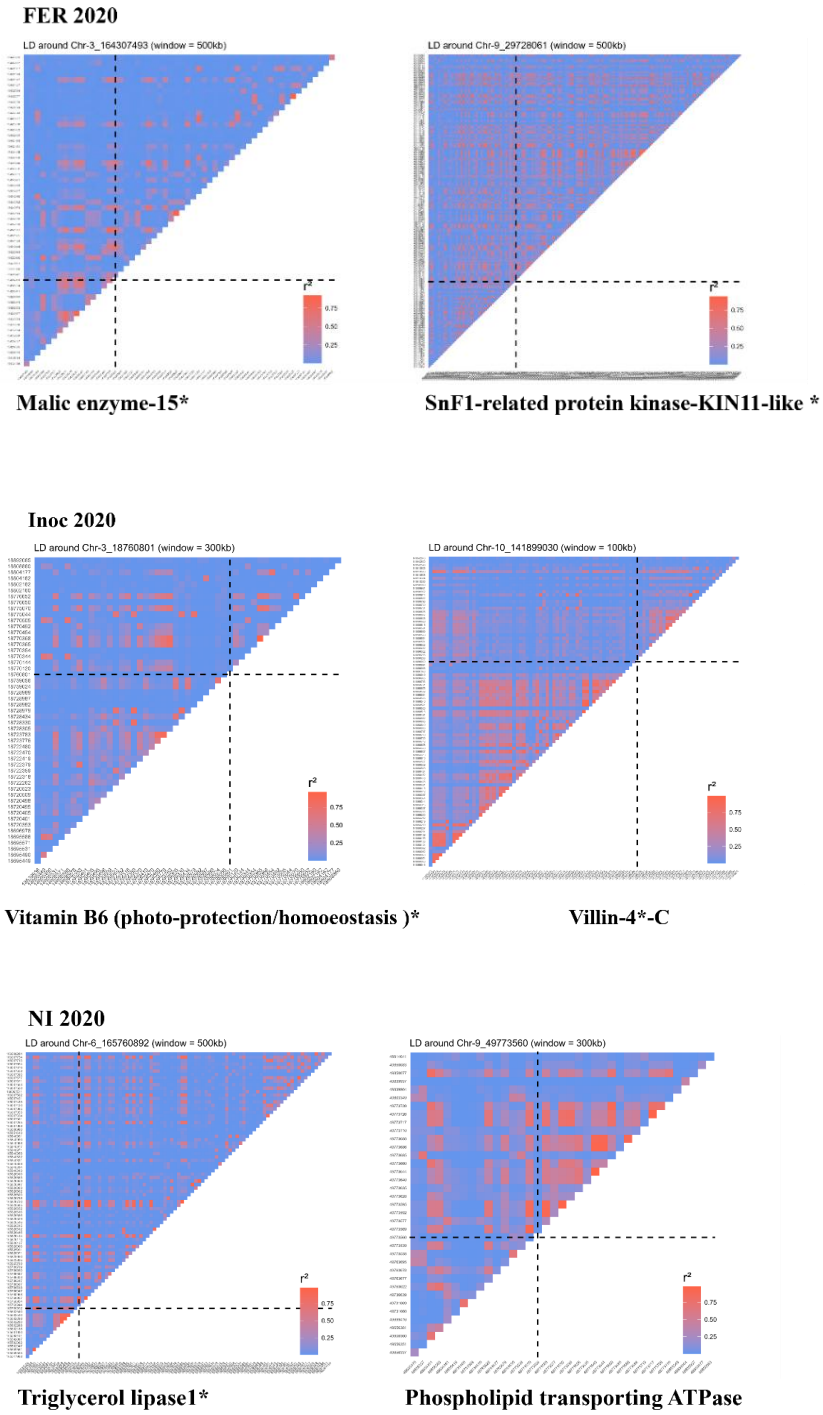

Figure S3. Local linkage disequilibrium (LD) patterns surrounding significant SNPs associated with FER resistance across year 2020. Local LD heatmaps (r^2) are shown for

genomic regions flanking the top SNPs identified in FER2020, Inoc2020, and NI2020. Each panel displays the LD structure within ±500 kb of the lead SNP (dashed line), warmer colors indicating stronger pairwise LD (higher r^2) (blue – weak LD, teal or pink –moderate LD and red-strong LD).Candidate genes located within high-LD windows around the associated SNPs are highlighted under each plot. Asterisks (*) indicate loci supported by local LD, and "C" denotes canonical defense-related genes.

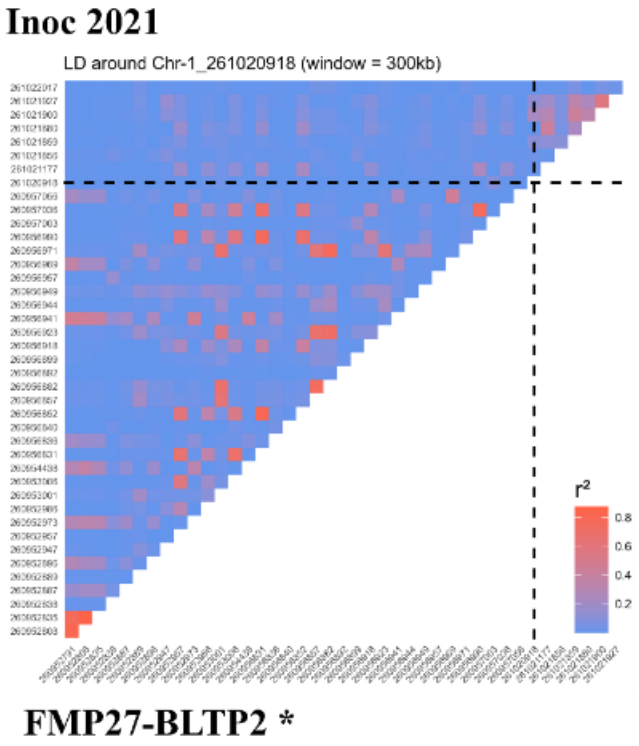

Figure S4. Local linkage disequilibrium (LD) patterns surrounding significant SNP associated with FER resistance across year 2021 (Inoc_2021).

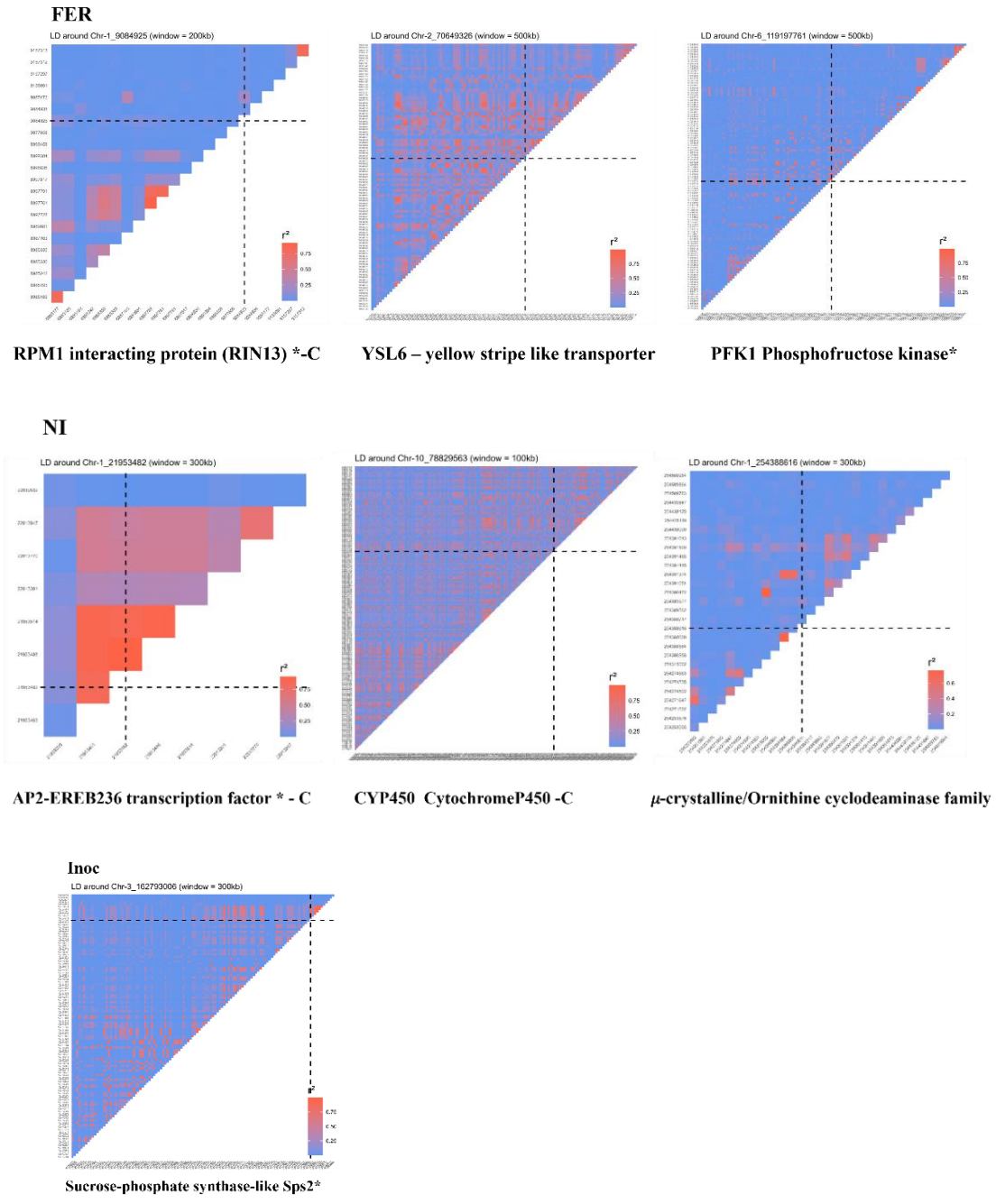

Figure S5. Local linkage disequilibrium (LD) patterns surrounding significant SNP associated with FER resistance across both years.

VITA

Sanskriti Acharya was born in Pyuthan and raised in Kathmandu, Nepal. She completed her B.Sc. (Honors) in Agriculture at HICAST, Purbanchal University. During an internship with the Nepal Agricultural Research Council (NARC), she researched on wheat spot blotch, evaluating the efficacy of *Trichoderma*-based biocontrols and commercial fungicides. Building on her interest in molecular approaches to crop disease resistance, she earned an M.S. in Entomology and Plant Pathology (Genomics & Bioinformatics concentration) at the University of Tennessee. Her master's research focused on genome-wide association studies (GWAS) to identify loci associated with resistance to Fusarium ear rot in a maize diversity panel, advised by Dr. Bode Olukolu. Her interests include quantitative genetics, bioinformatics pipelines, and translating genomic knowledge into practical breeding strategies.